University Library

A gateway to Melbourne's research publications

Minerva Access is the Institutional Repository of The University of Melbourne

Author/s:
Gransbury, GK;Boskovic, C

Title:
Valence Tautomerism in D‐Block Complexes

Citation:
Gransbury, G. K. & Boskovic, C. Valence Tautomerism in D‐Block Complexes. Encyclopedia of Inorganic and Bioinorganic Chemistry, pp.1-24. Wiley.

Persistent Link:
https://hdl.handle.net/11343/333721

Valence Tautomerism in d-block Complexes

Gemma K. Gransbury & Colette Boskovic

University of Melbourne, Parkville, VIC, Australia

1 Introduction 1
2 Fundamentals of Valence Tautomerism 1
3 Recent Advances in Valence Tautomerism 5
4 Computational Advances in Valence Tautomerism 16
5 Concluding Remarks 20
6 Abbreviations 20
7 Acknowledgments 21
8 Related Articles 21
9 References 21

1 INTRODUCTION

Nature masterfully uses the redox-activity of ligands to achieve many biological processes that are essential to life.[1] A simple example is oxygen transport and storage (as dioxygen or superoxide with Fe^{II} or Fe^{III}) by heme proteins. Inspired by nature, synthetic chemists have sought to exploit the redox-activity of ligands in metal complexes with a view to facilitating catalytic and stoichiometric chemical reactivity as well as for technology-based applications.[2–6] Coordinating redox-active metals to redox-active ligands can afford redox isomers with different charge distributions. In some cases, application of an external stimulus, such as heating/cooling or irradiation with visible light, induces reversible interconversion between the different electromeric forms of the metal complex. Such a stimulated and reversible intramolecular electron transfer between a redox-active metal and redox-active coordinated ligand is referred to as valence tautomerism (VT). A concerted spin transition at the metal center sometimes accompanies valence tautomeric electron transfer and the interconversions are phenomenologically related to spin crossover (SCO) and charge-transfer-induced spin transitions (CTISTs), also known as electron transfer coupled spin transitions (ETCSTs).[7–9] All three processes typically involve the same set of stimuli, the more common being temperature change and photoirradiation. Pressure variation, irradiation with X-rays, and application of an intense magnetic field are also known to stimulate these interconversions. While SCO is associated with a spin transition at a metal center, CTIST/ETCST involves intramolecular electron transfer between two metal ions, accompanied by a spin transition at one of the metal centers. VT is most well established for cobalt complexes of *ortho*-dioxolene ligands, involving an interconversion between low spin (LS) cobalt(III)-catecholate and high spin (HS) cobalt(II)-semiquinonate forms. VT is also known for cobalt complexes of other ligands as well as for compounds of 3d metals such as vanadium, manganese, iron, nickel and copper, and the 4d metal ruthenium.

Their different electronic structures typically confer different colors on the valence tautomeric forms of a metal compound. Being able to reversibly switch between species of different color affords thermo- and photochromic systems that can be interconverted by heating/cooling or light irradiation, which are relevant for application in displays or responsive materials. Combining the VT transitions with solvent guest-dependence may ultimately allow use as colorimetric vapor or gas sensors. Also of interest is the field of molecular electronics, which refers to the use of single molecules (or nanoscale ensembles of molecules) as electronic components such as rectifiers. Much effort has been dedicated to creating reproducible electrode-molecule-electrode junctions to measure the electrical/charge transport across single molecules.[10] Molecular switching associated with a VT transition can allow a valence tautomeric complex to function as a molecular logic gate, for instance, the single input and single output of a NOT logic operator can be the stimulus (heat, light) and response (magnetic or optical) of the switchable complex. Beyond the focus on charge in molecular electronics, the field of molecular spintronics is based on the use of electron spin of paramagnetic systems, as a degree of freedom in addition to charge, to process information.[11]

The last comprehensive review of VT appeared in 2014 in *Coordination Chemistry Reviews*.[12] Readers are also referred to prior reviews,[13–21] as well as to subsequent reviews addressing specific aspects of the field.[7,22–28] The scope of this article will be to cover the fundamental aspects and then focus on advances in the field of VT involving d-block metals since 2014.

2 FUNDAMENTALS OF VALENCE TAUTOMERISM

The most commonly studied VT systems are those with cobalt and *ortho*-dioxolene (diox) ligands (Figure 1). In these systems, cobalt may exist in the cobalt(II) or cobalt(III) oxidation state and the dioxolene is typically in the catecholate (cat^{2-}) or radical semiquinonate ($SQ^{\bullet-}$) oxidation state. Predominantly imine-based nitrogen-donor ancillary ligands are used, as they afford an appropriate ligand field to engender the LS cobalt(III) to HS cobalt(II) spin transition that accompanies the intramolecular electron transfer that is critical for the

Encyclopedia of Inorganic and Bioinorganic Chemistry, Online © 2011–2021 John Wiley & Sons, Ltd.
This article is © 2021 John Wiley & Sons, Ltd.
This article was published in the *Encyclopedia of Inorganic and Bioinorganic Chemistry* in 2021 by John Wiley & Sons, Ltd.
DOI: 10.1002/9781119951438.eibc2785

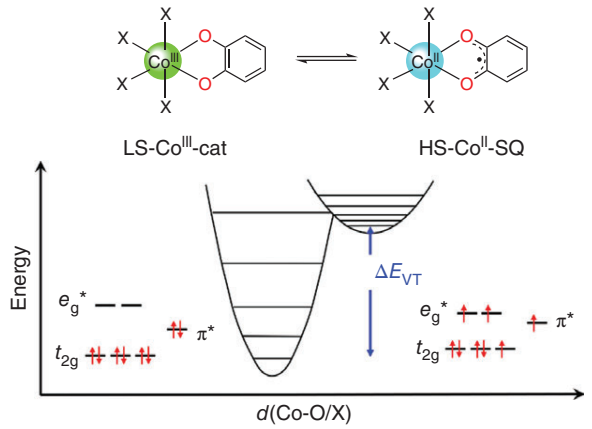

Figure 1 Valence tautomerism in a cobalt–dioxolene complex with corresponding electronic configurations and potential energy curves. The average Co-O/X (X most commonly N and O) bond length is represented by *d*

prevalence of VT in cobalt–dioxolene systems. Thus the VT equilibrium is

$$\text{LS-Co}^{\text{III}}\text{-cat} \leftrightarrows \text{HS-Co}^{\text{II}}\text{-SQ} \quad (1)$$

The filled t_{2g} orbitals in octahedral LS-Co^{III} give rise to short metal–ligand bond lengths of 1.8–2.0 Å, which increase by 0.11–0.23 Å as the VT transition populates the antibonding e_g* orbitals of HS-Co^{II}. The VT interconversion to the HS-Co^{II}-SQ state increases the number of unpaired electrons on both the cobalt and dioxolene, therefore increasing the overall magnetic moment. In the simplest case, the transition is from a diamagnetic LS-Co^{III}-cat compound to a paramagnetic HS-Co^{II}-SQ species. Thus cobalt–dioxolene valence tautomers can be differentiated based on metal–ligand bond lengths, dioxolene bond lengths, magnetic properties, and ultraviolet–visible–near-infrared (UV–Vis–NIR) spectral properties.

For thermally induced VT to occur in cobalt–dioxolene systems, the LS-Co^{III}-cat state must be thermodynamically more stable ($\Delta H_{VT} < 0$) and populated at low temperature. The HS-Co^{II}-SQ state has a larger entropy ($\Delta S_{VT} > 0$) than the LS-Co^{III}-cat state due to a higher spin state degeneracy and more closely spaced vibrational levels resulting from longer metal–ligand bonds. On increasing temperature, the entropic ($T\Delta S_{VT}$) component of the Gibbs free energy for the interconversion (ΔG_{VT}) will overcome the enthalpic (ΔH_{VT}) term and the HS-Co^{II}-SQ state will become the most stable. The thermal VT transition is characterized by the critical temperature ($T_{1/2}$) at which there are equal proportions of the two electromeric forms ($\Delta H_{VT} = T\Delta S_{VT}$).

Cobalt–dioxolene VT complexes can be broadly divided into two classes, with either one or two dioxolene ligands per cobalt. The complexes with two dioxolene ligands generally include one dioxolene in the semiquinonate oxidation state. Thus typical complexes include neutral [Co(diox)(SQ)(NL)$_2$] and [Co(diox)(SQ)(N$_2$L)] and monocationic [Co(diox)(N$_4$L)]$^+$ complexes featuring monodentate (NL), bidentate (N$_2$L) or tetradentate (N$_4$L) nitrogen-donor ancillary ligands. The first complex to exhibit thermally induced VT, [Co(3,5-dbdiox)(3,5-dbSQ)(bpy)] (bpy = 2,2′-bipyridine; 3,5-dbdiox = 3,5-di-*tert*-butyldioxolene; 3,5-dbSQ$^{\bullet-}$ = 3,5-di-*tert*-butylsemiquinonate), was reported by Buchanan and Pierpont in 1980.[29] Since then, many cobalt–dioxolene complexes have been found to exhibit thermally induced VT interconversions with $T_{1/2}$ values in solution and in the solid state ranging from 100 K to over 400 K. For all these complexes, the cobalt coordination environment remains pseudo-octahedral and the donor atoms are limited to oxygen atoms from the dioxolene units and nitrogen or sulfur atoms from ancillary ligands.

The second most widespread stimulus for inducing VT in cobalt–dioxolene systems is photoirradiation and compounds that exhibit a thermal interconversion sometimes also undergo a photoinduced transition. Some 16 years after the first report of thermally induced VT, pulsed laser photolysis studies on solutions of several [Co(diox)(SQ)(N$_2$L)] complexes indicated that irradiating with green light via a ligand to metal charge transfer (LMCT) band of the LS-Co^{III}-cat tautomer can afford a LMCT excited state, which relaxes to the transient HS-Co^{II}-SQ tautomer.[30] Picosecond spectroscopy at room temperature suggested that the HS-Co^{II}-SQ tautomer forms within the rise time of 90 ps and then relaxes back to the LS-Co^{III}-cat tautomer at a rate of 10^7–10^8 s^{-1}. After the discovery of the photoinduced spin transitions in solid samples of SCO and CTIST/ETCST complexes at low temperatures, it was found that VT interconversions can similarly be photoinduced in solid samples of cobalt–dioxolene complexes at cryogenic temperature (typically around 10 K) to give rise to long-lived metastable species.[31] Incomplete conversion is often observed, due to sample opacity and the overlap of transitions of the two valence tautomers giving rise to a photostationary state. The photoinduced HS-Co^{II}-SQ tautomer converts back to the original LS-Co^{III}-cat tautomer on heating, which is quantified by determining the temperature at which the thermal-magnetic susceptibility profile measured after irradiation rejoins the nonirradiated curve. For VT complexes, the "T_{LIVT}" measured in this way is in the range 38–90 K. A reverse photoinduced VT transition of the metastable photoinduced HS-Co^{II}-SQ tautomer back to LS-Co^{III}-cat tautomer can sometimes be achieved by irradiating the metal to ligand charge transfer (MLCT) band with red light.[32] In the low-temperature regime,

Encyclopedia of Inorganic and Bioinorganic Chemistry, Online © 2011–2021 John Wiley & Sons, Ltd.
This article is © 2021 John Wiley & Sons, Ltd.
This article was published in the *Encyclopedia of Inorganic and Bioinorganic Chemistry* in 2021 by John Wiley & Sons, Ltd.
DOI: 10.1002/9781119951438.eibc2785

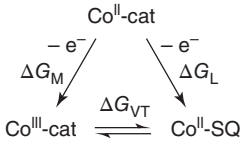

Figure 2 Relationship between cobalt–dioxolene redox states and Gibbs free energy for a VT transition

the lifetimes of the photoinduced tautomers are typically 10^4–10^5 s.

2.1 Redox Tuning: Electronic and Steric Effects

In principle, oxidation of a Co^{II}-cat species can result in ligand or metal oxidation. The Gibbs free energies of these processes (ΔG_L and ΔG_M for ligand and metal oxidation, respectively) are related to the Gibbs free energy of the VT transition (Figure 2) according to Equation (2):

$$\Delta G_{VT} = \Delta G_L - \Delta G_M \quad (2)$$

For thermally induced VT to occur, ΔG_{VT} must be close to zero and positive at low temperature and negative at high temperature. This can be achieved by minimizing the difference between the Gibbs free energies of the two processes, that is, matching the relevant redox potentials of the cobalt and dioxolene redox processes and therefore the energies of the corresponding molecular orbitals. The redox potential of the cobalt can be tuned via the non-redox-active ancillary ligand through a combination of electronic and steric effects. A family of ligands commonly used are those based on tris(2-pyridylmethyl)amine (tpa). Increasing the degree of methylation at the 6-position on the three pyridyl rings affords related ligands bis(2-pyridylmethyl)(6-methyl-2-pyridylmethyl)amine (Metpa), bis(6-methyl-2-pyridylmethyl)(2-pyridylmethyl)amine (Me_2tpa) and tris(6-methyl-2-pyridylmethyl)amine (Me_3tpa). For cobalt complexes with Me_ntpa ligands, increasing n from 0 to 3 increases the steric crowding around the metal center, stabilizing the longer bonds of the HS-Co^{II} state and decreasing the Co^{III}/Co^{II} redox potential. This effect can be employed to tune the charge distribution and VT transition temperature, for example in the family of complexes $[Co(3,5\text{-dbdiox})(Me_n\text{tpa})]^+$ (Figure 3).[33] The redox potential of the dioxolene ligand can also be tuned by the electronic properties of the ring substituents. Electron-withdrawing halogen substituents stabilize the catecholate form, while electron-donating *tert*-butyl derivatives favor the semiquinonate state.[34] The VT interconversion characteristics are also dependent on the electronic properties of the ancillary ligand. An example is the family of complexes $[Co(3,5\text{-dbdiox})(3,5\text{-dbSQ})(N_2L)]$, where the reduction potential

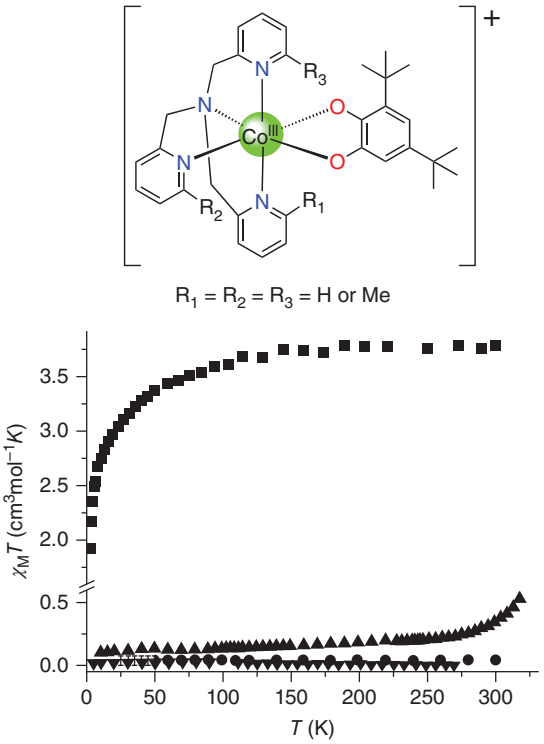

Figure 3 Structure and solid state magnetic susceptibility data for $[Co(3,5\text{-dbdiox})(Me_n\text{tpa})]^+$ (n = 0 (▼), 1 (●), 2 (▲) and 3(■)). [Beni *et al.* [33]].

of derivatized 2,2′-bipyridine ancillary ligands (N_2L), correlates with $T_{1/2}$ values, varying from less than 190 K to 348 K.[35]

2.2 Valence Tautomerism in Solution and the Solid State

In solution, thermally induced VT interconversions are generally measured by variable temperature electronic absorption (UV–Vis) spectroscopy or Evans NMR method magnetic susceptibility measurements. A gradual profile is typically evident due to the lack of cooperativity in solution. The $T_{1/2}$ is also often solvent-dependent, and although the origin of this is not clear cut, it appears to correlate with either the solvent polarity or donor number or arise from specific intermolecular interactions between solvent molecules and the metal complex.[36]

In the solid state, thermally induced VT interconversions may be abrupt or gradual and can be incomplete within the experimentally accessible temperature range.[37] These interconversions are commonly monitored by variable-temperature magnetic susceptibility measurements on bulk samples or variable temperature crystallography of single crystals. Interconversions may also display hysteresis, in which the value of a physical property, such as the product of the molar magnetic susceptibility and

Encyclopedia of Inorganic and Bioinorganic Chemistry, Online © 2011–2021 John Wiley & Sons, Ltd.
This article is © 2021 John Wiley & Sons, Ltd.
This article was published in the *Encyclopedia of Inorganic and Bioinorganic Chemistry* in 2021 by John Wiley & Sons, Ltd.
DOI: 10.1002/9781119951438.eibc2785

temperature ($\chi_M T$), depends on the history of the sample.[38] If the VT transition occurs at different temperatures on warming and cooling, the sample is bistable between these temperatures, which is important for potential applications.

In the solid state, the crystal packing can significantly affect the VT transition, modulating $T_{1/2}$, graduality, completeness, reversibility, stepwise nature and hysteresis, and potentially even suppressing the VT altogether.[39] Valence tautomeric transitions are generally found to be more abrupt in crystalline samples than in solution due to cooperativity. Cooperativity can result in the opening of hysteresis loops, such as for [Co(3,6-dbdiox)(3,6-dbSQ)(py_2O)] (where py_2O = bis(pyridyl)ether, 3,6-dbdiox = 3,6-di-*tert*-butyldioxolene; 3,6-dbSQ$^{\bullet-}$ = 3,6-di-*tert*-butylsemiquinonate), which undergoes a significant change in conformation of the ancillary ligand upon VT, resulting in a 230 K-wide hysteresis loop.[38] So-called "chemical pressure" arising from co-crystallized solvent molecules or counterions can also influence the nature of the VT transition by inhibiting the ability of the cobalt complex to undergo the molecular expansion that accompanies the low temperature to high temperature transition.[40] The loss of solvent on heating a crystalline sample is sometimes associated with different behavior on cooling the sample than on heating, but this is not hysteresis as subsequent heating-cooling cycles are superimposable.

2.3 Valence Tautomerism Across the d-Block

Thermally induced VT has been reported for complexes of various metals, including the p-block metal tin and f-block ytterbium, which are outside the scope of this article.[12] However, cobalt–dioxolene complexes constitute by far the majority of examples. Historically, another very important cobalt complex that exhibits thermally- and photo-induced VT is the homoleptic complex of the O,N,O′-tridentate Schiff-base ligand 3,5-di-*tert*-butyl-1,2-quinone-1-(2-hydroxy-3,5-di-*tert*-butylphenyl)-imine, which coordinates in the Cat-N-BQ$^-$ or radical Cat-N-SQ$^{\bullet 2-}$ oxidation states. The neutral complex [LS-Co^{III}(Cat-N-SQ)(Cat-N-BQ)] is obtained, which undergoes a VT interconversion to [HS-Co^{II}(Cat-N-BQ)$_2$] upon heating (Figure 4).[41] Dioxolene complexes of manganese have also been found to exhibit thermally induced VT in both solid state and solution. Two one-electron processes involving switching between three states can take place according to Equation (3)[42]:

$$Mn^{IV}\text{-(cat)}_2 \leftrightarrows \text{HS-}Mn^{III}\text{-(cat)(SQ)} \leftrightarrows \text{HS-}Mn^{II}\text{-(SQ)}_2 \quad (3)$$

Unlike the cobalt systems, spin transitions do not occur for manganese complexes. In addition, detection of the transition using magnetometry is prevented by the maintenance of the $S = 3/2$ ground state spin for each electromer due to antiferromagnetic coupling between the manganese ion and semiquinonate ligand. Manganese complexes with tridentate O,N,O′-donor Schiff base ligands have also exhibited VT interconversions.[43]

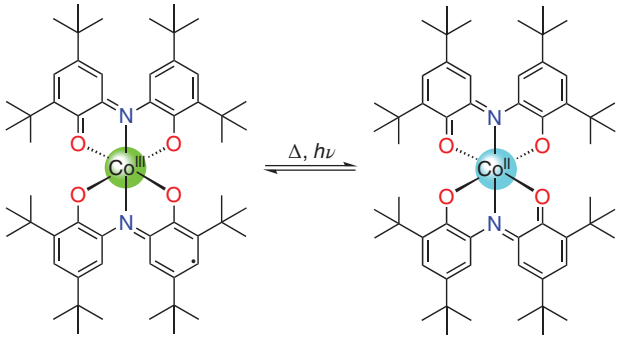

Figure 4 Valence tautomeric interconversion of [LS-Co^{III}(Cat-N-BQ)(Cat-N-SQ)] to [HS-Co^{II}(Cat-N-BQ)$_2$]. [Based on Evangelio *et al.*[41]]

A thermally induced VT interconversion has been reported for an iron–dioxolene complex according to[42]:

$$\text{HS-}Fe^{III}\text{-cat} \leftrightarrows \text{HS-}Fe^{II}\text{-SQ} \quad (4)$$

Again, unlike the cobalt systems, spin transitions do not occur in these iron complexes and the entropic driver for the VT transition is much less than for the analogous cobalt and manganese complexes due to the minimal difference in Fe—O bond distances between HS iron(II) and iron(III). Thermally induced VT has also been observed for complexes comprised of ferrocene units linked through a conjugated bridge to a perchlorotriphenylmethyl radical.[44] In the case of iron, these transitions can be conveniently monitored by variable temperature Mössbauer spectroscopy.

Thermally induced VT transitions are known for four coordinate copper dioxolene complexes according to[45]:

$$Cu^{II}\text{-cat} \leftrightarrows Cu^{I}\text{-SQ} \quad (5)$$

This chemistry is relevant to the biological role of copper-based oxidoreductase enzymes.[1] Chemically assisted VT has been reported for nickel dioxolene complexes, although this involves a change of coordination number due to solvent coordination and does not fall within the strict definition of VT.[46] Finally, there have been some reports of ruthenium dioxolene complexes existing in an equilibrium between Ru^{III}-SQ and Ru^{II}-BQ (BQ = benzoquinone) or Ru^{II}-SQ and Ru^{I}-BQ analogs.[47] Long-standing non-dioxolene examples of thermally induced VT include polynuclear nickel and copper complexes with multidentate polyimine or N,O-donor Schiff base ligands.[48,49]

Encyclopedia of Inorganic and Bioinorganic Chemistry, Online © 2011–2021 John Wiley & Sons, Ltd.
This article is © 2021 John Wiley & Sons, Ltd.
This article was published in the *Encyclopedia of Inorganic and Bioinorganic Chemistry* in 2021 by John Wiley & Sons, Ltd.
DOI: 10.1002/9781119951438.eibc2785

3 RECENT ADVANCES IN VALENCE TAUTOMERISM

3.1 Mononuclear Valence Tautomeric Compounds

3.1.1 Cobalt–Dioxolene complexes

A number of new examples of $[Co(diox)(SQ)(NL)_2]$ complexes have been found to display thermally induced VT in recent years (Table 1). Panja, Mathonière, and coworkers reported the cis and trans isomers of $[Co(Br_4diox)(Br_4SQ)(py)_2]^+$ (py = pyridine; Br_4diox = tetrabromodioxolene; $Br_4SQ^{\bullet-}$ = tetrabromosemiquinonate) can be interconverted by dissolution in different solvents.[50] The cis isomer is the kinetic product and the trans isomer is the thermodynamic product. Solid samples of the pyridinium salts exhibit thermally induced VT interconversions with $T_{1/2} > 300$ K influenced by desolvation and packing effects. VT can be used to direct unusual reactivity: in subsequent work, *trans*-$[Co(Br_4diox)(Br_4SQ)(py)_2]^+$ was found to undergo VT-driven nucleophilic substitution.[60] Aromatic nucleophilic substitution of a bromo group with a pyridyl group on each dioxolene afforded *trans*-$[Co^{III}(Br_3pycat)_2(py)_2]^+$ (Br_3pycat^{2-} = 3,5,6-tribromo-4-pyridiniumcatecholate). Pinheiro *et al*. carried out detailed variable temperature structural studies to probe the effect of solvation and crystal packing on the cooperativity of VT interconversions in the previously reported *trans*-$[Co(4\text{-}NO_2\text{-}py)_2(3,5\text{-}dbdiox)_2]$ and *trans*-$[Co(4\text{-}CN\text{-}py)_2(3,5\text{-}dbdiox)_2]$ (4-NO_2-py = 4-nitropyridine; 4-CN-py = 4-cyanopyridine).[54,61] The degree of cooperativity correlates with intermolecular hydrogen bonding between cobalt complexes. Overgaard, Iverson, and coworkers performed variable temperature crystallographic studies that revealed thermally induced VT for *trans*-$[Co(3,5\text{-}dbdiox)_2(3,5\text{-}di\text{-}BrPy)_2]$ and *trans*-$[Co(3,5\text{-}dbdiox)_2(3,5\text{-}di\text{-}ClPy)_2]$ (3,5-di-BrPy = 3,5-dibromopyridine; 3,5-di-ClPy = 3,5-dichloropyridine), while analogues with 3,4,5-tribromopyridine or 3,4,5-trichloropyridine ancillary ligands remained in the HS-Co^{II}-SQ form at all temperatures.[51]

VT has also been reported for several new $[Co(diox)(SQ)(N_2L)]$ compounds (Table 1). Thermal and light-induced VT was observed for $[Co(3,5\text{-}dbdiox)_2(bpym)]$ (bpym = 2,2′-bipyrimidine) by Bogani *et al*. (solid state $T_{1/2} = 215$ K; $T_{LIVT} = 68$ K).[55] Bubnov and coworkers described thermally induced VT for solid [Co(4-OMe-3,6-dbdiox)$_2$(1,10-phen)]·tol (1,10-phen = 1,10-phenanthroline; 4-OMe-3,6-dbdiox = 4-methoxy-3,6-di-*tert*-butyl-dioxolene) ($T_{1/2} = 254$ K).[56] Use of an alternative diaza-functionalized iminopyridine ancillary ligand afforded $[Co(3,6\text{-}dbdiox)_2(4\text{-}N\text{-}TEMPO\text{-}ip)]$ (4-*N*-TEMPO-ip = [2,2,6,6-tetramethyl-4-[[(*E*)-pyridin-2-ylmethylidene]amino]*cyclo*-hexyl]oxidanyl).[62] This compound exhibits

Table 1 Critical temperatures for recent mononuclear cobalt dioxolene VT compounds

Compound	$T_{1/2}$ (K) solid	$T_{1/2}$ (K) solution[(a)]	Ref
[Co(diox)(SQ)(NL)$_2$]			
cis-[pyH][Co(Br$_4$diox)(Br$_4$SQ)(py)$_2$]·MeOH	>300	—	50
trans-[pyH][Co(Br$_4$diox)(Br$_4$SQ)(py)$_2$]·2H$_2$O·2C$_3$H$_6$O	>300	—	50
trans-[Co(3,5-dbdiox)(3,5-dbSQ)(3,5-di-BrPy)$_2$]	245	—	51
trans-[Co(3,5-dbdiox)(3,5-dbSQ)(3,5-di-BrPy)$_2$]·tol	150	—	51
trans-[Co(3,5-dbdiox)(3,5-dbSQ)(3,5-di-ClPy)$_2$]·tol	150	—	51
trans-[Co(3,5-dbdiox)(3,5-dbSQ)(4-papy)$_2$]	396	—	52
trans-[Co(3,5-dbdiox)(3,5-dbSQ)(4-stypy)$_2$]	394	299 (toluene)	53
cis-[Co(3,5-dbdiox)(3,5-dbSQ)(4-stypy)$_2$]	397	287 (toluene)	53
trans-[Co(3,5-dbdiox)(3,5-dbSQ)(4-NO$_2$-py)$_2$]·tol	205	—	54
trans-[Co(3,5-dbdiox)(3,5-dbSQ)(4-NO$_2$-py)$_2$]·C$_6$H$_6$	128(↓), 162(↑)	—	54
trans-[Co(3,5-dbdiox)(3,5-dbSQ)(4-CN-py)$_2$]·tol	221	—	54
trans-[Co(3,5-dbdiox)(3,5-dbSQ)(4-CN-py)$_2$]·C$_6$H$_6$	240	—	54
[Co(diox)(SQ)(N$_2$L)]			
[Co(3,5-dbdiox)(3,5-dbSQ)(bpym)]	215	—	55
[Co(4-OMe-3,6-dbdiox)(4-OMe-3,6-dbSQ)(1,10-phen)]·tol	254	—	56
[Co(3,6-dbdiox)(3,6-dbSQ)(4-*N*-TEMPO-ip)]	220(↓), 270(↑)	—	62
[Co(diox)(N$_4$L)]$^+$			
[Co(Br$_4$diox)(Me$_3$tpa)]PF$_6$·1.2tol	>360	291 (DCM), 295 (DCE), 359 (MeCN)	34
[Co(Br$_4$diox)(Me$_3$tpa)]BPh$_4$	>360	—	34
[Co(3,5-dbdiox)(AzaNiPr)]	>350	300 (DCE), 320 (DBE), >300 (MeCN)	57
[Co(3,5-dbdiox)(pbqa)]PF$_6$	>350	—	58
[Co(Andiox)(Metpa)]PF$_6$	>400	—	59
[Co(Andiox)(Me$_2$tpa)]PF$_6$	>300	—	59

[(a)]DBE, 1,2-dibromoethane; DCE, 1,2-dichloroethane; DCM, dichloromethane; MeCN, acetonitrile.

Encyclopedia of Inorganic and Bioinorganic Chemistry, Online © 2011–2021 John Wiley & Sons, Ltd.
This article is © 2021 John Wiley & Sons, Ltd.
This article was published in the *Encyclopedia of Inorganic and Bioinorganic Chemistry* in 2021 by John Wiley & Sons, Ltd.
DOI: 10.1002/9781119951438.eibc2785

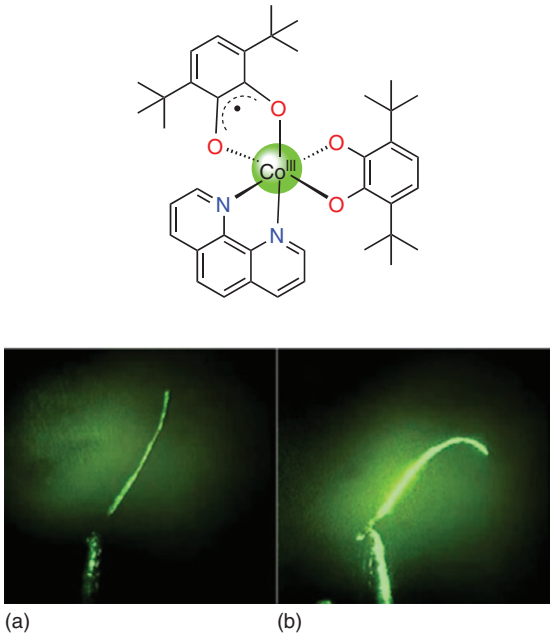

Figure 5 Photomechanical bending response to a green laser (532 nm) beam (a, without light; b, irradiated) of a crystal of [Co(3,6-dbdiox)(3,6-dbSQ)(1,10-phen)]. Temperature: 254 K. [Based on Bubnov *et al.*[63]]

a hysteretic thermally induced VT interconversion below room temperature. Bubnov *et al.* recently found that especially grown crystals of [Co(3,6-dbdiox)$_2$(1,10-phen)] can be reversibly and elastically bent upon laser irradiation or heating (Figure 5).[63] The thermal crystal bending occurs around the usual $T_{1/2}$ temperature and it is possible to tune this temperature by making solid solutions of varying composition with [Co(3,6-dbdiox)$_2$(bpy)].

New [Co(diox)(N$_4$L)]$^+$ VT complexes have also been reported (Table 1). Synthesized on the basis of density functional theory (DFT) calculated predictions (Section 4.2), Boskovic and coworkers found thermally induced VT for the PF_6^- and BPh_4^- salts of [Co(Br$_4$diox)(Me$_3$tpa)]$^+$ above 360 K in the solid state. Thermally induced VT was observed in solution in some solvents with solvent-dependent $T_{1/2}$ value (Table 1), while others preferentially stabilized one or the other charge distributions. Combined variable temperature electronic absorption spectroscopy and Evans NMR method magnetic susceptibility measurements suggest the following trend for $T_{1/2}$: dichloromethane < 1,2-dichloroethane < acetone ≈ acetonitrile < toluene. This study also explicitly described the relationship between the separation between the frontier metal and ligand-based redox processes, as measured by voltammetry, and the likelihood of being able to access a thermally induced VT interconversion at readily accessible temperatures. The same group also reported thermally induced VT for the isopropyl analogue of the [Co(3,5-dbdiox)(AzaNR)]$^+$ (AzaNR = *N*,*N*′-di-alkyl-2,11-diaza[3.3]-(2,6)pyridinophane) family of complexes,[57] in contrast to the SCO transition previously reported for the *tert*-butyl analogue.[64] Measurements performed in solution in different solvents again found that the $T_{1/2}$ shifts significantly with solvent, increasing in the order 1,2-dichloroethane < 1,2-dibromoethane < acetonitrile. Interestingly for both [Co(Br$_4$diox)(Me$_3$tpa)]$^+$ and [Co(3,5-dbdiox)(AzaNiPr)]$^+$ complexes, halogenated solvents preferentially stabilize the HS-Co^{II}-SQ tautomer, which may be due to specific intermolecular solvent–complex interactions.

Suenaga and coworkers described thermally induced VT in solid state and solution for [Co(3,5-dbdiox)(pbqa)](PF$_6$) (pbqa = (2-pyridylmethyl)bis(2-quinolylmethyl)amine)).[58] This is in contrast to the bpqa (bis(2-pyridylmethyl)(2-quinolylmethyl)amine) and tqa (tris(2-quinolylmethyl)amine) analogues, which are temperature invariant [LS-Co^{III}(3,5-dbcat)(bpqa)](PF$_6$) and [HS-Co^{II}(3,5-dbSQ)(tqa)](PF$_6$) up to 380 K in the solid state.

The nature of the magnetic coupling between the HS-Co^{II} ion and coordinated semiquinonate ligand has been unclear for some time, due to complications in modeling this system because of the significant unquenched orbital angular momentum of octahedral HS-Co^{II} ions. A recent combined theoretical and experimental investigation from Boskovic, Soncini, and coworkers has revealed the extreme sensitivity of the coupling to the geometry in each particular system.[65] For the case of [Co(3,5-dbSQ)(Me$_3$tpa)](PF$_6$)·tol, detailed investigation indicated dominant ferromagnetic exchange of similar magnitude to the anisotropy parameters of the cobalt(II) ion with a significant contribution from spin–orbit coupling.

3.1.2 *Cobalt Complexes with Redox-Active Ligands Other Than Dioxolenes*

In a departure from dioxolene ligands Brook and coworkers have investigated possible VT for a cobalt complex with tridentate dipyridyl verdazyl ligands.[66] The compound [Co(dipyvd)$_2$](PF$_6$) (dipyydH = 1-isopropyl-3,5-dipyridyl-6-oxoverdazyl) displays thermally induced VT in acetonitrile solution according to variable temperature magnetic susceptibility and visible absorption spectroscopic studies, interconverting between [LS-Co^{III}(dipyvd$^-$)(dipyvd$^\bullet$)]$^{2+}$ and [HS-Co^{II}(dipyvd$^\bullet$)$_2$]$^{2+}$ tautomers (Figure 6). The compound remains in the [HS-Co^{II}(dipyvd$^\bullet$)$_2$]$^{2+}$ form in the solid state at accessible temperatures.

Encyclopedia of Inorganic and Bioinorganic Chemistry, Online © 2011–2021 John Wiley & Sons, Ltd.
This article is © 2021 John Wiley & Sons, Ltd.
This article was published in the *Encyclopedia of Inorganic and Bioinorganic Chemistry* in 2021 by John Wiley & Sons, Ltd.
DOI: 10.1002/9781119951438.eibc2785

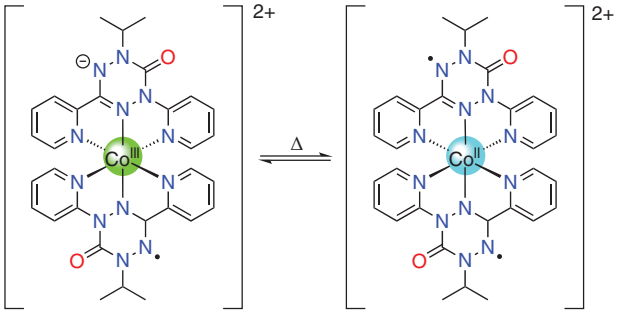

Figure 6 Valence tautomeric interconversion [LS-Co^{III}(dipyvd$^-$)(dipyvd$^{\bullet}$)]$^{2+}$ and [HS-Co^{II}(dipyvd$^{\bullet}$)$_2$]$^{2+}$.[66] [Fleming *et al*.[66]]

3.1.3 *Vanadium, Manganese, Iron, Copper, and Osmium Complexes*

Thermally induced VT was reported by Bendix and Clark for a bis(arylimino)acenaphthene (BIAN) vanadium complex.[67] In the solid state, the PF_6^- salt of the homoleptic complex [V(3,5-Me_2-BIAN)$_3$]$^+$ (3,5-Me_2-BIAN = *N*,*N*′-bis(3,5-dimethylphenylimino)acenaphthylene) exists in the [V^V(3,5-Me_2-BIAN^{2-})(3,5-Me_2-BIAN$^{\bullet-}$)$_2$]$^+$ form below 150 K, interconverting to [V^{IV}(3,5-Me_2-BIAN$^{\bullet-}$)$_3$]$^+$ above 150 K according to magnetic susceptibility data.

Panja and coworkers have proposed that the thermally induced VT interconversion from [Mn^{III}(Br_4cat)$_2$(py)]$^-$ to [Mn^{II}(Br_4SQ)(Br_4cat)(py)]$^-$ in methanol induces aromatic nucleophilic substitution of a Br_4cat^{2-} ligand by pyridine. This ultimately affords [Mn^{III}(Br_4cat)(Br_3pycat)(py)$_2$], which was characterized crystallographically.[68] This group subsequently reported a similar in situ formation of the Br_3pycat^- ligand for related cobalt complexes.[60]

New iron valence tautomeric compounds include [Fe^{III}(L_1)$_2$][BF_4] and [Co^{III}(η^5-$C_{10}H_{15}$)$_2$][Fe^{III}(L_1)$_2$] (L_1H_2 = 2-(2-phenylazo)-anilino-4,6-di-*tert*-butylphenol) reported by Mukherjee and coworkers.[69] The O,N,N-donor azo-appended *o*-amidophenolates can exist in the amidophenolate (AP^{2-}), iminobenzosemiquinonate ($ISQ^{\bullet-}$), and iminobenzoquinonate (IBQ) forms. Multiple physical techniques and DFT calculations indicate thermally dependent VT equilibria involving [LS-Fe^{III}(L_1^{ISQ})$_2$]$^+$ and [LS-Fe^{II}(L_1^{IBQ})(L_1^{ISQ})]$^+$ tautomers for [Fe^{III}(L_1)$_2$]$^+$ and [LS-Fe^{III}(L_1^{AP})$_2$]$^-$ and [LS-Fe^{II}(L_1^{ISQ})(L_1^{AP})]$^-$ for [Fe^{III}(L_1)$_2$]$^-$.

Bröring *et al*. have described a fascinating family of bis(pyridyl-imino)isoindoline (bpi) iron(III) complexes [Fe(4-R-bpi)$_2$] with different substituents at the 4-position of the pyridine rings.[70] Characterization with multiple physical techniques indicates that the R = H, Me, and Et analogs remain in the temperature-independent HS iron(II) state, and the R = *t*-Bu analogue exhibits a thermal SCO. In contrast, the R = OMe analogue is oxidized to iron(III) and, in the solid state, exhibits a thermally induced VT interconversion and accompanying spin transition between [LS-Fe^{II}(bpi$^-$)(bpi$^{\bullet 2-}$)] and [HS-Fe^{III}(bpi$^-$)$_2$].

Lehnert, Dey, and coworkers performed a detailed multi-technique study revealing thermally induced VT for synthetic models of cytochrome P450 in THF (Figure 7).[71] Low-temperature spectroscopic data of thiolate-bound iron complexes that fit the description of the cytP450 active site are best described as thiolate-bound HS ferric porphyrins. However, upon heating, a thiyl-radical bound ferrous species becomes evident and is present in significant amounts in solution at room temperature. These redox isomers can be reversibly interchanged at room temperature by the addition or removal of water to the apolar medium. The presence of the ferrous thiyl state helps explain the high sensitivity of synthetic thiolate-bound ferric porphyrin mimics of cytP450 toward dioxygen, which is not exhibited by ferric porphyrins with redox innocent axial ligands, as well as their instability toward a free radical like nitric oxide.

Himmel *et al*. have investigated a series of guanidino-substituted aromatic redox-active ligands in copper complexes. They have reported thermally induced VT for [Cu(L_2)X_2]PF_6 (L_2 = 5,6-bis-(*N*,*N*′-dimethyl-*N*,*N*′-ethylene-guanidino)-2,2-dimethyl-[1,3]-benzodioxole; X = Cl, Br) in MeCN solution.[72] The {Cu^{II}-L_2^0} species is favored at lower temperature, interconverting to a {Cu^I-$L_2^{\bullet+}$} tautomer at higher temperature.

There are some indications for thermally induced VT for the copper compound [Cu(L_3)$_2$][PF_6] (L_3H_2 = (2-[2-(benzylthio)phenyl-amino]-4,6-di-*tert*-butylphenol) described by Mukherjee and coworkers.[73] The O,N,S-donor *o*-amidophenolate ligand can exist in the amidophenolate, $ISQ^{\bullet-}$ and IBQ forms and bind bi- or tridentate. Variable temperature NMR and X-ray photoelectron (XPS) spectroscopy suggests thermally dependent VT equilibria with [Cu^I(L_3^{IBQ})$_2$]$^+$ and at low temperature interconverting into [Cu^{II}(L_3^{IBQ})(L_3^{ISQ})]$^+$ upon heating.

Extension of VT to the 5d metals has recently been reported for the aminophenolate osmium complex [Os($^{OX}L_4$)Cl(PPh_3)$_2$] ($^{OX}L_4H_2$ = *N*-(benzophenoxazine)-*o*-aminophenol).[74] Variable temperature electron paramagnetic resonance (EPR) spectra in dichloromethane suggest thermally induced VT between the Os^{III}(L_4^{2-}) form at low temperature and Os^{II}($L_4^{\bullet-}$) at room temperature. No such interconversion is evident for the ruthenium analogue.

3.2 Polynuclear Valence Tautomeric Compounds

3.2.1 *Dinuclear Complexes*

Dinuclear valence tautomeric complexes are mainly of interest for the possibility of accessing two-step transitions and therefore three-state molecular switches, as

Encyclopedia of Inorganic and Bioinorganic Chemistry, Online © 2011–2021 John Wiley & Sons, Ltd.
This article is © 2021 John Wiley & Sons, Ltd.
This article was published in the *Encyclopedia of Inorganic and Bioinorganic Chemistry* in 2021 by John Wiley & Sons, Ltd.
DOI: 10.1002/9781119951438.eibc2785

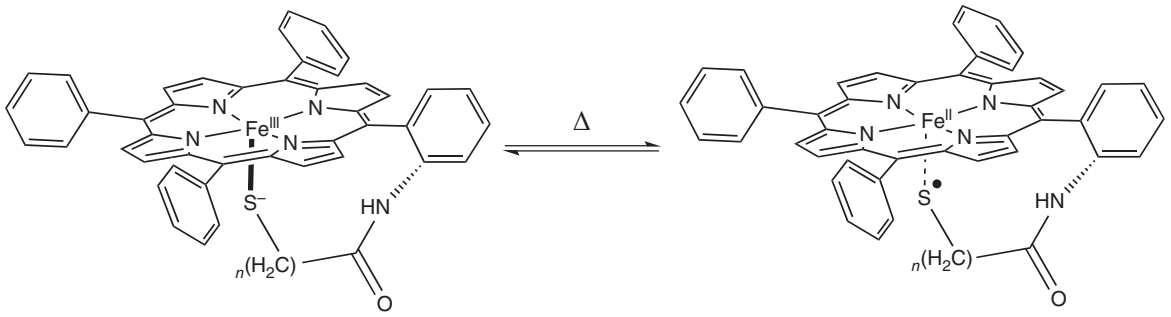

Figure 7 Valence tautomeric equilibrium for cytochrome P450 model compounds. [Das *et al.*[71]]

is possible with dinuclear iron(II) SCO systems.[75–77] In terms of material applications, more extensive chromatic responses may be available, and for molecular electronics, three-state switches offer the possibility of more complex logic gates. A number of dinuclear cobalt complexes have been synthesized and investigated. Two alternative approaches have been employed, making use of either ancillary or redox-active ligands to bridge the metal centers. Bridging redox-active ligands have generally been either tetraoxolene or bis-dioxolene species.

One of the most exciting early breakthroughs with dinuclear VT complexes was the room temperature hysteresis with a loop with of 13 K reported by Sato *et al.* for the tetraoxolene-bridged cobalt compound $[\{Co(tpa)\}_2(\mu\text{-dhbq})](PF_6)_3$ (dhbq = 2,5-dihydroxy-1,4-benzoquinone) in 2006.[78] The thermal transition involves the one-electron VT interconversion:

$$\{\text{LS-Co}^{\text{III}}\text{-dhbq}^{\bullet 3-}\text{-LS-Co}^{\text{III}}\} \leftrightarrows \{\text{HS-Co}^{\text{II}}\text{-dhbq}^{2-}\text{-LS-Co}^{\text{III}}\} \quad (6)$$

Sato and coworkers attributed the wide hysteresis to significant intermolecular interactions in the form of offset $\pi\cdots\pi$ interactions of the pyridine rings of the tpa ancillary ligands and an edge-to-face interaction between the tpa pyridine rings and the $dhbq^{3-}$ benzene rings. The same group subsequently confirmed the importance of the crystal packing and intermolecular interactions in generating the hysteretic transition, reporting a polymorph with different packing that exhibits a much higher $T_{1/2}$ and no apparent hysteresis.[79] The new polymorph also exhibits poorer photo-induced VT properties and a lower T_{LIVT}.

Building on Sato's work, Yu, Li, and coworkers described how replacing the original PF_6^- counteranion by AsF_6^- decreases the width of the magnetic hysteresis accompanying the thermal VT transition for $[\{Co(tpa)\}_2(dhbq)](AsF_6)_3$.[80] The change is presumably due to changes in the crystal packing influencing the cooperativity of the transition. In contrast, replacement of the tetradentate tpa ancillary ligands with two bidentate ligands stabilizes the $\{\text{HS-Co}^{\text{II}}\text{-dhbq}^{2-}\text{-LS-Co}^{\text{III}}\}$ state and eliminates VT behavior for the compounds $[\{Co(N_2L)_2\}_2(dhbq)](PF_6)_3$ (N_2L = bpy and 2,2′-bipyridyl amine).[81] Efforts to extend the VT family by replacing the tetraoxolene ligand with isoelectronic O_2N_2-donor bis-bidentate bridging ligands is yet to afford complexes that display VT.[82]

On looking to bis-dioxolene bridging ligands, another highlight from past work is the establishment by the Boskovic group of two-step VT interconversions for $[\{Co(Me_2tpa)\}_2(spiro)]^{2+}$ ($spiroH_4$ = 3,3,3′,3′-tetramethyl-1,1′-spirobis(indane)-5,5′,6,6′-tetrol; Figure 8) of the form:

$$\{\text{LS-Co}^{\text{III}}\text{-cat-cat-LS-Co}^{\text{III}}\} \leftrightarrows \{\text{LS-Co}^{\text{III}}\text{-cat-SQ-HS-Co}^{\text{II}}\} \leftrightarrows \{\text{HS-Co}^{\text{II}}\text{-SQ-SQ-HS-Co}^{\text{II}}\} \quad (7)$$

in both solid and solution states.[84] The two-step nature of the transition was attributed to the weak but nonzero electronic communication between the two cobalt–dioxolene moieties mediated by the spirocyclic carbon that links the two dioxolene units in the bridging ligand. This work was followed by a subsequent study from the same group employing the related Br_4spiro ($Br_4spiroH_4$ = 3,3,3′,3′-tetramethyl-1,1′-spirobi(indan)-4,4′,7,7′-tetrabromo-5,5′,6,6′-tetraol) bis-dioxolene ligand to bridge the cobalt centers.[83] Detailed experimental and DFT computational studies (Section 4.2) allowed elucidation of thermodynamic parameters governing the one- and two-step VT behavior in bis(dioxolene)-bridged dinuclear cobalt complexes. The presence of a VT interconversion and the VT transition profile, that is, one concerted two-electron step, two distinct one-electron steps, or an incomplete or partial transition, can be rationalized by (i) the degree of electronic communication within the bis(dioxolene) ligand and (ii) the matching of cobalt and dioxolene redox potentials. The correlation is valid for the complexes with spiroconjugated bis(dioxolene) bridging ligands investigated in these studies, as well as for literature dinuclear cobalt complexes with nonspiroconjugated bis(dioxolene) bridging ligands.[12]

Encyclopedia of Inorganic and Bioinorganic Chemistry, Online © 2011–2021 John Wiley & Sons, Ltd.
This article is © 2021 John Wiley & Sons, Ltd.
This article was published in the *Encyclopedia of Inorganic and Bioinorganic Chemistry* in 2021 by John Wiley & Sons, Ltd.
DOI: 10.1002/9781119951438.eibc2785

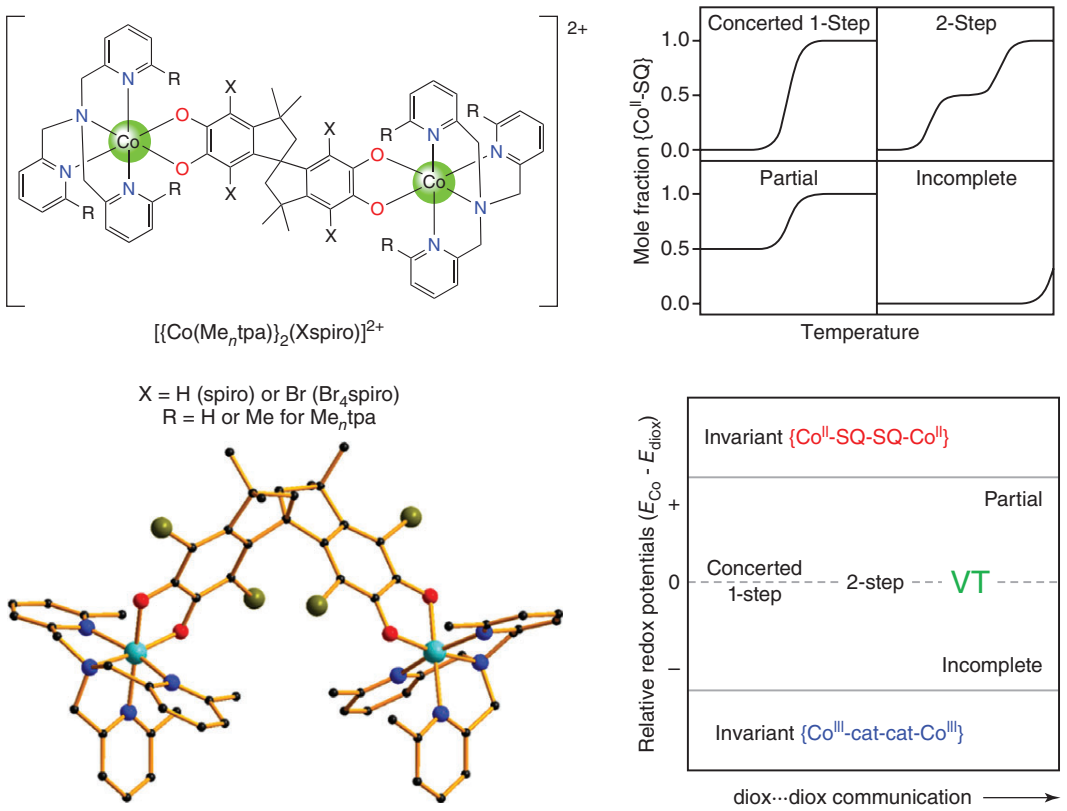

Figure 8 Clockwise from top left: structural representation of [{Co(Me$_n$tpa)}$_2$(Xspiro)]$^{2+}$; schematic of valence tautomeric transitions in dinuclear cobalt–bis(dioxolene) complexes showing the possible profiles of concerted one-step, two-step, partial, and incomplete transitions; the relationship between the transition profile of a complex to its electronic communication and redox properties and X-ray structure of [{Co(Me$_3$tpa)}$_2$(Br$_4$spiro)]$^{2+}$. [Gransbury *et al.*[83]]

Bubnov and coworkers employed the alternative approach of bridging cobalt centers through the non redox-active ancillary ligand, reporting three dinuclear cobalt complexes with bridging bis-bidentate N-donor ligands of general formula [{Co(diox)$_2$}$_2$(OMP)] (diox = 3,6-dbdiox, 3,6-di-*tert*-butyl-4-Cl-*o*-benzoquinone (4-Cl-3,6-dbdiox) or 3,6-di-*tert*-butyl-4,5-*N*,*N*′-piperazino-o-benzoquinone (4,5-pip-3,6-dbdiox); OMP = 2,2′-(pyridine-2,6-diyl)bis(N1,N1,N3,N3-tetramethylpropane-1,3-diamine)).[85] The three complexes each exhibit concerted two-electron VT interconversions according to solid state magnetic susceptibility data with $T_{1/2}$ values around 200 K. The concerted nature of the interconversion is consistent with minimal electronic communication through the bridging ligand.

As part of a series of studies on guanidino-substituted aromatic redox-active ligands in copper complexes, Himmel and coworkers reported the first dinuclear copper complex to exhibit VT [{CuCl$_2$}L$_5$], which features 2,3,5,6-tetrakis(tetramethyl-guanidino)pyridine (L$_5$) as a bridging redox-active ligand.[86] The thermally induced VT interconversion is evident in acetone solution and involves two-electron transfer and interconversion of a {Cu^{II}-L$_5^0$-Cu^{II}} species with a neutral bridging ligand at low temperature to a {Cu^{I}-L$_5^{2+}$-Cu^{I}} species with a dicationic bridging ligand at room temperature (Figure 9). The equilibrium is solvent dependent, with more polar solvents favoring the copper(I) species. Intriguingly, the equilibrium is also dependent on the concentration of [(*n*-Bu)$_4$N]PF$_6$ in dichloromethane.

3.2.2 *Trinuclear Complexes*

The novel radical-bridged trinuclear compound [Co$_3$(L$_6$)(3,5-dbdiox)] (L$_6^{\bullet-}$ = 3,6-bis(2-pyridyl)-1,2,4,5-tetrazine radical) (Figure 10) was reported by Li, Zhuang, Zhou, and coworkers to undergo a thermally induced VT transition.[87] Magnetic susceptibility studies indicate a complete interconversion from [Co$^{III}_3$(μ_2-L$_6$)$_3$(3,5-dbcat)$_3$] to the [Co$^{II}_3$(μ_2-L$_6$)$_3$(3,5-dbSQ)$_3$] tautomer at 390 K, which is irreversible due to loss of crystallinity. DFT calculations suggest that flipping of the tetrazine radical spins is integral to the VT interconversion.

Encyclopedia of Inorganic and Bioinorganic Chemistry, Online © 2011–2021 John Wiley & Sons, Ltd.
This article is © 2021 John Wiley & Sons, Ltd.
This article was published in the *Encyclopedia of Inorganic and Bioinorganic Chemistry* in 2021 by John Wiley & Sons, Ltd.
DOI: 10.1002/9781119951438.eibc2785

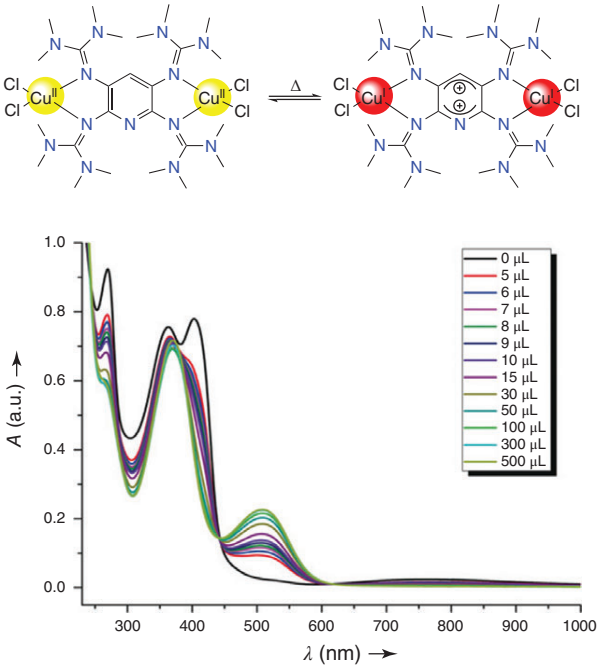

Figure 9 Two-electron VT interconversion for dinuclear [{$CuCl_2$}L_5] in acetone and variation of the electronic absorption spectra corresponding to the different valence tautomeric forms upon addition of [(*n*-Bu)$_4$N]PF_6 in dichloromethane. [Wiesner *et al.*[86]]

3.3 Multifunctional Valence Tautomeric Compounds

Teki and coworkers have described efforts towards multifunctional VT by functionalizing dioxolene ligands with anthracene and boron-dipyrromethene (BODIPY) moieties.[59,88] The charge distribution of the compounds [Co(Me$_n$tpa)(Andiox)]PF_6 (n = 0–3; Andiox = 9-(3,4-di-hydroxyphenyl)anthracene) and [Co(Me$_n$tpa)(An-BODIPY-diox)]PF_6 (n = 0 and 3; An-BODIPY-diox = 9-(3,4-dihydroxyphenyl)-10-[4,4-difluoro-1,3,5,7-tetramethyl-8-(phenyl)-4-bora-3a,4a-diaza-*s*-indacene]anthracene) is controlled by the degree of methylation of the Me$_n$tpa ligand. Compounds [Co(Me$_n$tpa)(Andiox)]PF_6 (n = 1 and 2) exhibit thermally and photo-induced VT and a possible antenna effect from the anthracene.[59] The room temperature BODIPY fluorescence in the An-BODIPY-diox compounds is modulated by the charge distribution across the cobalt–dioxolene unit, which is attributed to enhancement of nonradiative decay processes based on the stronger metal–ligand interactions for the LS-Co^{III}-cat tautomer.

Typical VT was reported for *trans*-[Co(3,5-dbdiox)(3,5-dbSQ)(4-papy)] (4-papy = 4-phenylazopyridine) by Khusniyarov and coworkers.[52] Partial dissociation in solution affords a five-coordinate complex in equilibrium with free 4-papy ligand and addition of extra 4-papy drives the

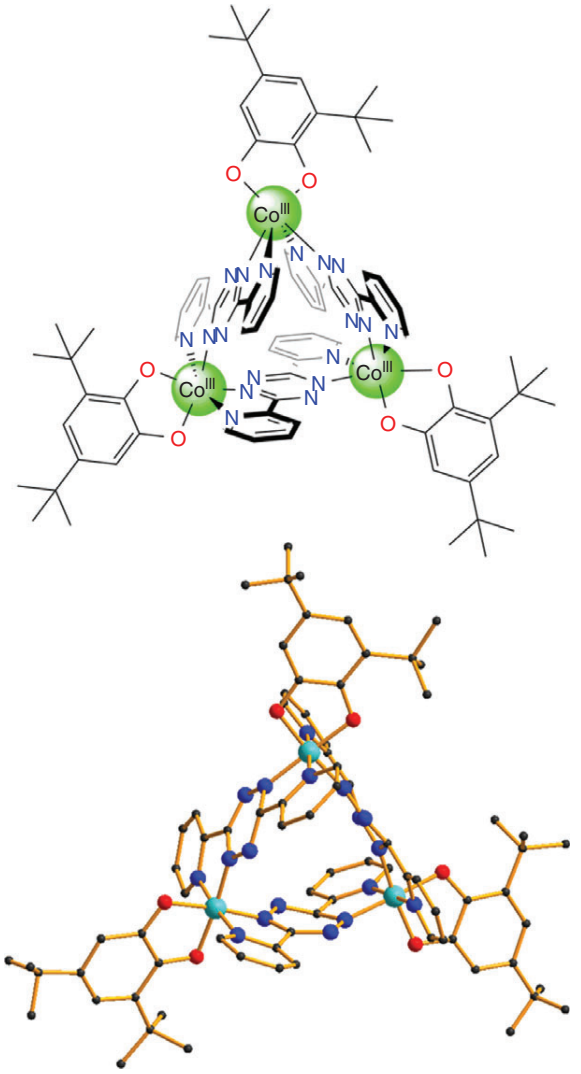

Figure 10 Representations of [$Co^{III}{}_3(L_6)_3$(3,5-dbcat)$_3$].[87] [Based on Li *et al.*[87]]

equilibrium back to the six-coordinate VT complex. The use of *trans*- or *cis*-4-styrylpyridine (*trans*-4-stypy, *cis*-4-stypy) instead affords *trans*- and *cis*-[Co(3,5-dbdiox)(3,5-dbSQ)(4-stypy)], both of which display thermally induced VT in the solid state and in solution, with solution (solid) $T_{1/2}$ = 299 (394 K) and 287 K (397 K), for trans and cis complexes, respectively.[53] The 4-styrylpyridine ligands are *cis-trans* photoisomerizable and bidirectional trans ↔ cis interconversion of the compounds can be achieved at room temperature via UV photoirradiation in toluene or benzene solution. The bidirectional photo-induced trans ↔ cis interconversion also induces a VT transition, with the trans isomer in the LS-Co^{III}(cat) and the cis isomer in the HS-Co^{II}(SQ) state. The photo-induced interconversion appears to proceed via a five-coordinate intermediate following

Encyclopedia of Inorganic and Bioinorganic Chemistry, Online © 2011–2021 John Wiley & Sons, Ltd.
This article is © 2021 John Wiley & Sons, Ltd.
This article was published in the *Encyclopedia of Inorganic and Bioinorganic Chemistry* in 2021 by John Wiley & Sons, Ltd.
DOI: 10.1002/9781119951438.eibc2785

dissociation of one of the 4-stypy ligands. It was found that after irradiating the solutions for around one hour, no further change was evident in the composition of the solution and the photoswitching is incomplete in both directions, always affording mixture of the two isomers. However, these systems represent the first example of room temperature photoswitchable VT to give long-lived products.

A similar approach by Frank and coworkers involved utilization of a photoisomerizable spirooxazine-functionalized phenanthroline-based ancillary ligand (Figure 11).[89] Thin films of the compound [Co(3,5-dbdiox)(3,5-dbSQ)(APSO)] (APSO = 4-methylspiro[4-aza-homoadamantane-5,2′-[2H-1,4]ox-azino-[2,3-f][1,10]phenanthroline) can be interconverted between four states around room temperature, involving the closed spirooxazine and open photomerocyanine forms of the ancillary ligand. The photoinduced structural change initiates a reversible VT process at the cobalt–dioxolene unit. The optical gating process is described as a photoisomerization-induced spin–charge excited state (PISCES). The photo-induced state is relatively long-lived (τ = 10 s at 300 K) and governed by the lifetime of the metastable state of the photochromic ligand.

Sato and coworkers reported the use of a VT interconversion to induce polarization switching in the carefully designed heterodimetallic polar compounds [(Cr(*SS*-cth))(Co(*RR*-cth))(μ-dhbq)]$(PF_6)_2Cl$ and [(Cr(*RR*-cth))(Co(*SS*-cth))(μ-dhbq)]$(PF_6)_2Cl$ (cth = 5,5,7,12,12,14-hexamethyl-1,4,8,11-tetraazacyclotetradecane.[90] Use of symmetric (*SS*-*RR*) pairs of the enantiopure ancillary cth ligands affords polar structures. The thermally induced VT interconversion is the heterometallic version of Equation (6), that is:

$$\{\text{LS-Co}^{\text{III}}\text{-dhbq}^{\bullet 3-}\text{-Cr}^{\text{III}}\} \leftrightarrows \{\text{HS-Co}^{\text{II}}\text{-dhbq}^{2-}\text{-Cr}^{\text{III}}\} \quad (8)$$

Between 300 and 400 K, the transition is hysteretic and engenders a change in the dipole moments of the complexes. The VT and resulting polarization change could also be induced by irradiation with visible light at 7 K. This compound represents an example of a unique method of inducing polarization switching arising from the intramolecular electron transfer associated with thermally- or photo-induced VT interconversion, rather than the more usual ion displacement. A subsequent study by Sato and coworkers involved incorporation of the racemic *rac*-cth ancillary ligand in the complex [Co(phendiox)(*rac*-cth)]$^+$ (phendioxH_2 = 9, 10-dihydroxyphenanthrene) affording a macroscopic polarization change accompanying both thermally- and photo-induced VT interconversion.[91] The

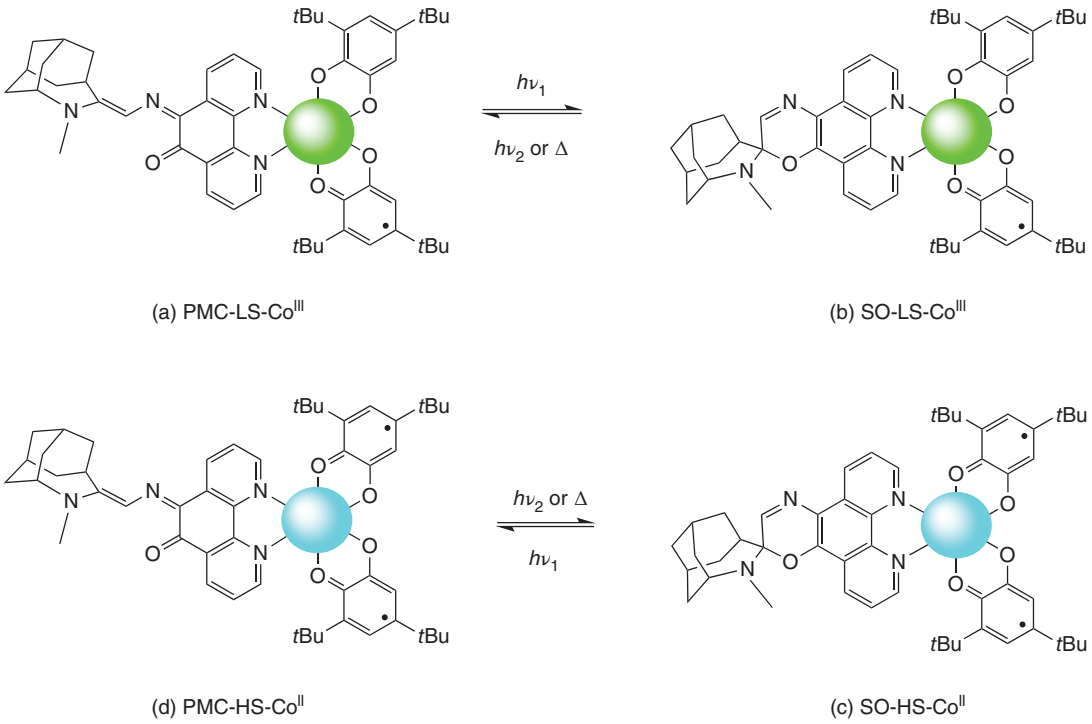

Figure 11 Four possible electronic states of [Co(3,5-dbdiox)$_2$(APSO)] are formed by a combination of open (PMC) and closed (SO) states of the photochrome and the low-spin d^6 Co^{III} and high-spin d^7 Co^{II} states of the cobalt–dioxolene. Light irradiation involves visible green light (hν_1) or UV light (hν_2). Thermal VT interconverts pairs of states (b) and (c), and (a) and (d). Photoisomerization-Induced Spin–Charge Excited State (PISCES) interconverts states (a) and (c). [Paquette *et al.*[89]]

Encyclopedia of Inorganic and Bioinorganic Chemistry, Online © 2011–2021 John Wiley & Sons, Ltd.
This article is © 2021 John Wiley & Sons, Ltd.
This article was published in the *Encyclopedia of Inorganic and Bioinorganic Chemistry* in 2021 by John Wiley & Sons, Ltd.
DOI: 10.1002/9781119951438.eibc2785

compound crystallizes in a polar space group, which allows the direct observation of the accumulative change of the dipole moments on the single-crystal level, leading to the observation of a pyroelectric current. This electronic pyroelectricity is completely different to more commonly observed ferroelectricity in that the materials are polarized without the requirement for an applied electric field.

3.4 Valence Tautomerism in Coordination Polymers

Incorporating valence tautomeric units into coordination polymers (CPs) is of interest for several reasons. Linking the switchable units through covalent bonds can enhance the cooperativity of the transition and potentially favor hysteresis and bistability for devices. Three-dimensional CPs, or metal–organic frameworks (MOFs) also offer the possibility of inclusion of guest molecules in pores or channels within the structure, which can modulate the characteristics of the VT transition. These materials thus have potential as colorimetric, and potentially selective, sensors for gas or solvent molecules.

VT has been observed for 1D, 2D, and 3D CPs and MOFs. Valence tautomeric CPs based on cobalt were reviewed in 2018, along with cobalt SCO CPs.[25] Numerous neutral 1D chains of general formula [Co(diox)(SQ)(NLN)] (NLN = ditopic N-donor linking ligand) have been found to exhibit thermal and photo-induced VT.[92–98] It has also proved possible to link cobalt–dioxolene VT moieties via the redox-active ligand into 1D CPs.[99]

Employment of the tetradentate polypyridyl ligand tetrakis(4-pyridyloxymethylene)methane (tpom) affords the 2D CP $[\{Co(3,5\text{-dbdiox})(3,5\text{-dbSQ})\}_2(tpom)]$, where the tpom acts as a 4-connecting linker.[100] This compound exhibits both thermally and photo-induced VT, but no hysteresis.

An exciting breakthrough is the 2D manganese CP reported by Luneau and coworkers that displays VT accompanied by significant hysteresis around room temperature (Figure 12).[101] Variable temperature magnetic and spectroscopic studies revealed that the manganese-nitronyl-nitroxide compound $[Mn_2(NITIm)_3]ClO_4$ (NITImH = 2-(2-imidazolyl)-4,4,5,5-tetramethyl-4,5-dihydro-1H-3-oxide-1-oxyl) undergoes thermally induced VT involving oxidation of the manganese(II) ions to manganese(III) as two of the three deprotonated ($NITIm^{\bullet-}$) radical ligands are reduced to the diamagnetic aminoxyl form. The $T_{1/2}$ values are 287 and 274 K upon heating and cooling, respectively. Subsequent work by these authors showed analogs with BF_4^- and PF_6^- anions undergo a two-step transition via a mixed-valence $Mn^{II}Mn^{III}$ state.[102] The ClO_4^- and BF_4^- compounds show an increase of ~40 K in their transition temperatures and retain hysteresis at an external pressure of 0.1 GPa.[103]

Tetraoxolene ligands are well known as linkers in 2D "honeycomb" layered CPs. Thermally induced VT was described by Miyasaka and coworkers for the iron-tetraoxolene compound $(NPr_4)_2[Fe_2(Cl_2An)_3]\cdot 2acetone\cdot H_2O$ (Cl_2AnH_2 = chloranilic acid).[104] While a $[(HS\text{-}Fe^{III})_2(Cl_2An^{2-})(Cl_2An^{\bullet 3-})_2]^{2-}$ tautomer is favored at low temperature, heating induces interconversion to a $[(HS\text{-}Fe^{II})(HS\text{-}Fe^{III})(Cl_2An^{2-})_2(Cl_2An^{\bullet 3-})]^{2-}$ tautomer with a $T_{1/2}$ of 236 K. This material is also multifunctional, with the low temperature state showing

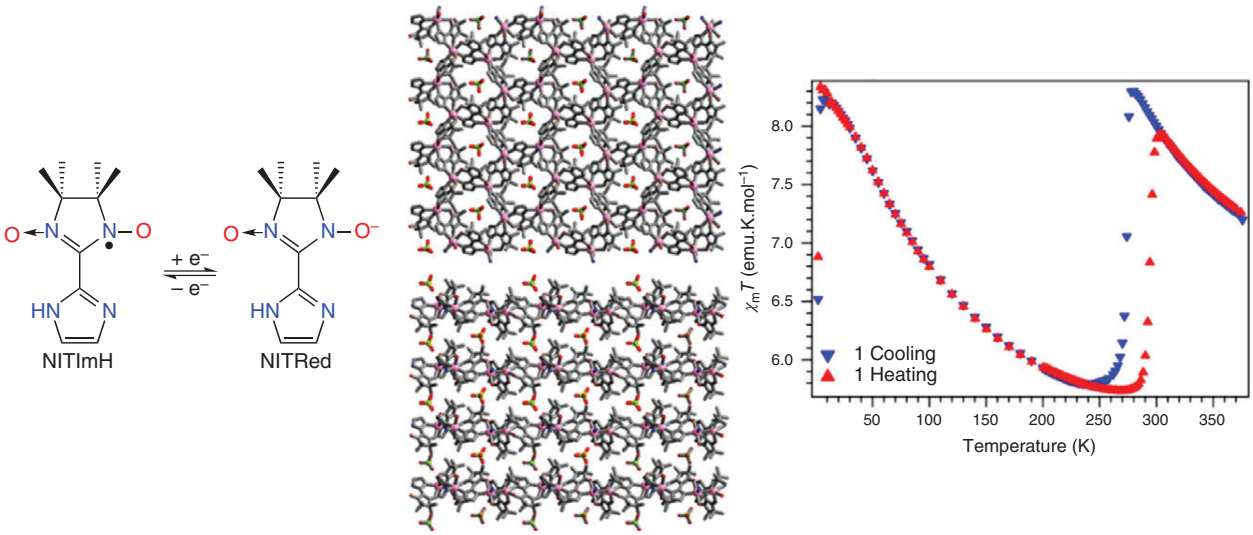

Figure 12 Nitronyl-nitroxide NITIm ligands, two views of the honeycomb layered structure of 2D VT CP $[Mn_2(NITIm)_3]ClO_4$ and the magnetic susceptibility hysteresis associated with the VT interconversion above 250 K. The increase in $\chi_M T$ upon cooling below 200 K is attributed to magnetic coupling between Mn^{II} ions and the radical ligands. [Lannes *et al.*[101]]

Encyclopedia of Inorganic and Bioinorganic Chemistry, Online © 2011–2021 John Wiley & Sons, Ltd.
This article is © 2021 John Wiley & Sons, Ltd.
This article was published in the *Encyclopedia of Inorganic and Bioinorganic Chemistry* in 2021 by John Wiley & Sons, Ltd.
DOI: 10.1002/9781119951438.eibc2785

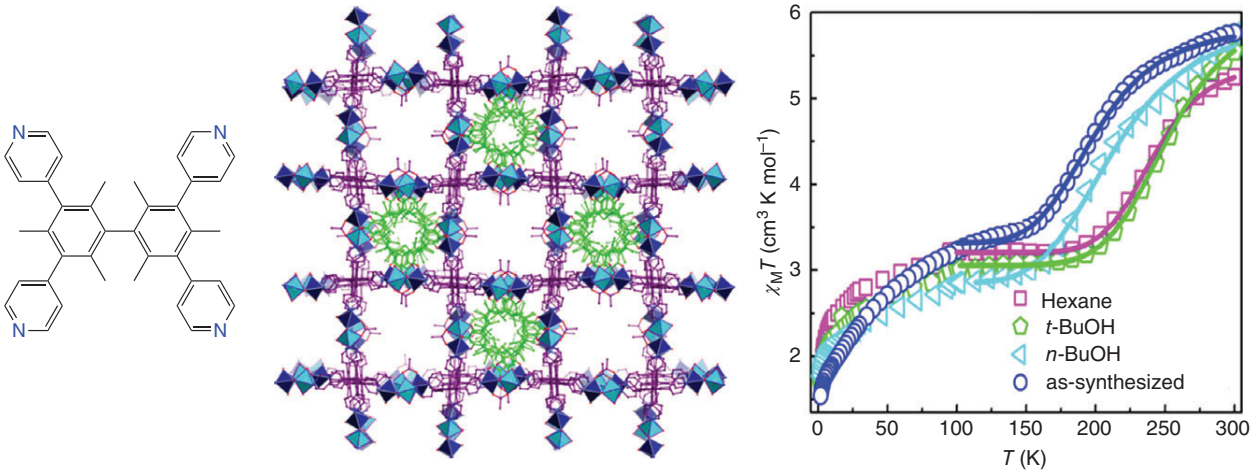

Figure 13 Linking 3,3′,5,5′-tetrakis(4-pyridyl)bimesityl ligand (L_7), structure and dependence of magnetic susceptibility hysteresis on guest molecules for [$Co_2(O_2CMe)$(3,5-dbdiox)(3,5-dbcat)(L_7)]. [Based on Li *et al.*[105]]

ferrimagnetic ordering of HS-Fe^{III} and $Cl_2An^{\bullet 3-}$ in 1D chains leading to magnetic hysteresis up to 5 K and single chain magnetic behavior.

A recent highlight is the 3D tetradentate polypyridyl cobalt–dioxolene MOF reported by Li, Zhuang and Zhou, and coworkers (Figure 13).[105] In this compound, the tetradentate polypyridyl ligand 3,3′,5,5′-tetrakis (4-pyridyl)bimesityl (L_7) serves as a 4-connecting linker of dinuclear {$Co^{II}Co^{III}(O_2CMe)$(3,5-dbdiox)(3,5-dbcat)} building blocks, affording the 3D MOF [$Co_2(O_2CMe)$(3,5-dbdiox)(3,5-dbcat)(L_7)]. Magnetic susceptibility studies indicate that the VT $T_{1/2}$ value can be tuned by the presence of different solvent molecules as guests in the pores of the MOF. These observations provide proof of concept for the use of valence tautomeric MOFs as solvent sensors.

3.5 Valence Tautomeric Nanoparticles and Microparticles

Constructing 1D CPs from valence tautomeric units has subsequently led to incorporation of these CPs into micro- and nanoparticles with a view to applications.[24,25] Most of the relevant work has come from Ruiz-Molina, Hernando, Novio and coworkers.[25] Amorphous valence tautomeric micro- and nanoparticles have been fabricated from 1D VT cobalt–dioxolene CPs with particle size ranging from tens of nanometers to a few microns.[106] Variation of both the bridging and dioxolene ligands, as well as the polymerization conditions, allows tuning of the properties of the product particles. Hydrophobic VT nanoparticles constructed from 1D cobalt–dioxolene CPs were achieved by functionalizing catechol ligands with long alkyl chains and exhibit enhanced thermal and colloidal stability.[107] Another class of these particles exhibit pH tuning of the stability and therefore VT transition arising from interactions with an imine functionality in the bis-dioxolene linking ligand.[108] Small magnetic hysteresis associated with the VT transition has been observed for amorphous spherical nanoparticles comprised of cobalt–dioxolene CPs with a mixed bridging ligand that combines catecholate and pyridine units.[99]

A fascinating alternative approach to microstructured valence tautomeric materials has been to incorporate the molecular [Co^{III}(Cat-N-BQ)(Cat-N-SQ)]/[Co^{II}(Cat-N-BQ)$_2$] complex within a liquid-filled core of a polyamide microcapsule.[109] The cobalt complex is included in toluene solution via interfacial polymerization. Changing the solvent in the core allows tuning of the temperature of the thermal VT transition. In a step towards application in devices, the liquid-filled microcapsules were embedded in polyvinylalcohol films with retention of the thermal VT. The VT interconversion of the microparticles could be followed both by variable temperature magnetometry and by monitoring particle color change with an optical microscope.

3.6 Valence Tautomeric Compounds in Thin Films and on Surfaces

In an alternative approach to generating valence tautomeric materials for devices, Ruiz-Molina and coworkers fabricated flexible thin films of [Co^{III}(Cat-N-BQ)(Cat-N-SQ)]/[Co^{II}(Cat-N-BQ)$_2$] (Figure 4) doped into poly(methyl methacrylate) (PMMA) via drop casting (Figure 14).[110] The transparent thin films with 2% doping exhibited thermally induced interconversions akin to those in solution. As the percentage of doping is increased above 2%, the cobalt compound exhibits a tendency to crystallize. The success of the [Co^{III}(Cat-N-BQ)(Cat-N-SQ)]/[Co^{II}(Cat-N-BQ)$_2$] doped PMMA films and particles was followed by deposition of this composite onto silicon surfaces

Encyclopedia of Inorganic and Bioinorganic Chemistry, Online © 2011–2021 John Wiley & Sons, Ltd.
This article is © 2021 John Wiley & Sons, Ltd.
This article was published in the *Encyclopedia of Inorganic and Bioinorganic Chemistry* in 2021 by John Wiley & Sons, Ltd.
DOI: 10.1002/9781119951438.eibc2785

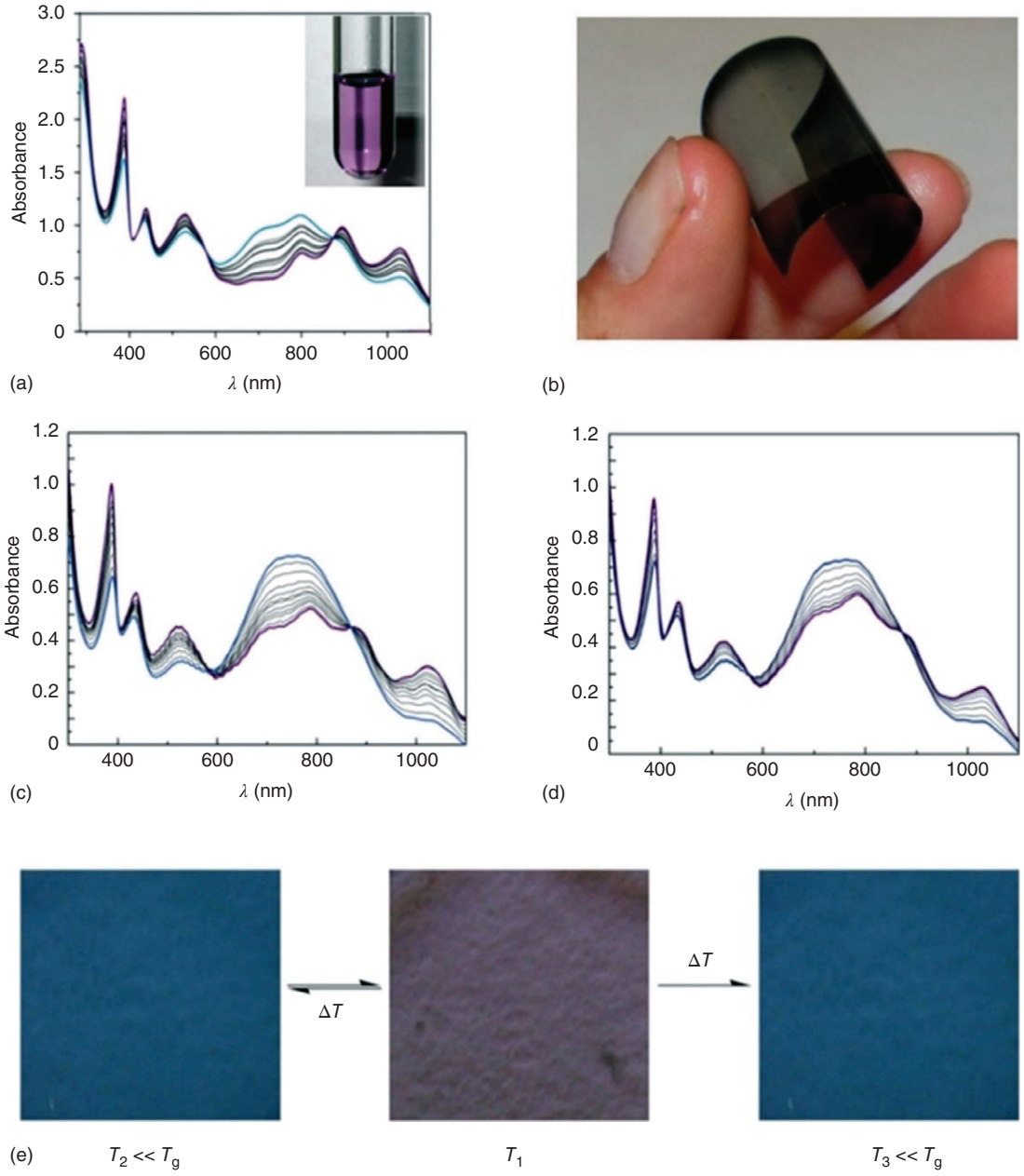

Figure 14 Studies of $[Co^{III}(Cat\text{-}N\text{-}BQ)(Cat\text{-}N\text{-}SQ)]/[Co^{II}(Cat\text{-}N\text{-}BQ)_2]$: (a) variable-temperature (200–350 K) UV–Vis spectra of a toluene solution (Inset: image of the solution at room temperature); (b) image of a flexible PMMA thin-film containing 2% wt.; (c) variable-temperature (heating 163–373 K) UV–Vis spectra of the thin-film shown in (b); (d) variable-temperature (cooling 373–163 K) UV–Vis spectra of the thin-film shown in (b) [Novio *et al.*[110]]; (e) photographs of a 2% wt. PMMA thin film at different temperatures (T_1 is room temperature, $T_g = 395$ K).

by means of different lithographic techniques.[110] Both dip-pen nanolithography and nanoimprint lithography afforded functionalized surfaces. Variable temperature diffuse reflectance spectra of these surfaces indicate that the VT properties remain upon surface deposition.

To take a step back, the earliest efforts towards deposition of VT compounds on surfaces were reported by Shultz and coworkers in 2005.[111] Functionalization of a bipyridyl ancillary ligand with a mercapto group allowed binding of mononuclear cobalt–dioxolene complexes on gold nanoparticles. Evaporation of films afforded tethering through the mercapto group with variable temperature infrared spectroscopy indicating retention of the thermal VT interconversion.

Encyclopedia of Inorganic and Bioinorganic Chemistry, Online © 2011–2021 John Wiley & Sons, Ltd.
This article is © 2021 John Wiley & Sons, Ltd.
This article was published in the *Encyclopedia of Inorganic and Bioinorganic Chemistry* in 2021 by John Wiley & Sons, Ltd.
DOI: 10.1002/9781119951438.eibc2785

Subsequently, Poneti, Mannini, and coworkers grafted a monolayer of thiol-derivatized VT complexes [Co(Me_2tpa)(dbdioxSH)]$^+$ (dbdioxSH = 4,6-di-*tert*-butyl-3-((4-(mercaptomethyl)benzyl)thio)benzene-1,2-hydroxydioxolene) and non-VT analogues [Co(Me_ntpa)(dbdioxSH)]$^+$ (n = 0 and 3), onto a polycrystalline gold surface.[112] X-ray absorption spectroscopy of the monolayers indicated that the charge distributions and thermal and photo-induced VT interconversions were similar to the free complexes. The retention of the molecular switchability on grafting to a metallic surface is an important result from the perspective of future applications in molecular devices.

The deposition of cobalt–dioxolene VT CPs on gold surfaces has also been pursued by Ruiz-Molina and coworkers.[24,113,114] Initial efforts employed nanoparticles comprised of 1D cobalt–dioxolene CPs with carboxylic acid-functionalized dioxolene ligands.[113] A carbodiimide-mediated coupling reaction with an amino-functionalized gold surface generated deposited nanoparticles. Variable temperature XPS spectroscopy confirmed maintenance of the thermally induced VT interconversion. A highly creative alternative approach pursued by the same research group involved atomic force microscope (AFM) assisted lithography and synthesis of a cobalt–dioxolene CP within femtoliter droplets deposited on gold surfaces.[114] Adjacent tips of the same AFM were separately filled with the metal salt and organic ligand and these solutions were sequentially delivered to the same position on the surface. This method reproducibly afforded spherical CP nanostructures with control over the positioning on the surface. The surface nanostructures were characterized by grazing angle infrared and micro Raman spectroscopy to confirm formation of the cobalt–dioxolene CP. The very small quantities of the compounds in the surface array made it difficult to characterize any VT; however, this work provides an important proof of feasibility for this novel AFM-assisted lithographic approach to surface functionalization.

3.7 Advances in Techniques for Measuring Valence Tautomerism

Valence tautomeric interconversions involve a significant change in molecular and electronic structure of the metal coordination unit. The structural change confers significant difference in a range of physical and spectroscopic properties exhibited by the two tautomers. Thus, depending on the specific situation, VT can be monitored by a range of experimental techniques, including solid and solution state magnetic susceptibility, single crystal and powder diffraction, X-ray emission, infrared, UV–Vis, and X-ray absorption spectroscopy, as well as EPR, near-infrared (NIR) and Mössbauer spectroscopy. Typically, thermally induced VT is monitored by variable temperature measurements, while photo-induced VT is monitored following an experimental response to irradiation with visible light of an appropriate wavelength. The few examples of pressure-influenced VT have involved monitoring thermal VT transitions by magnetic susceptibility or X-ray absorption spectroscopy upon application of external pressure.[115–118]

One recent advance in experimental techniques for monitoring thermally induced VT was reported by Liang, Gaffney, and coworkers. These researchers investigated the classic compounds [Co(3,5-dbdiox)(3,5-dbSQ)(N_2L)] (N_2L = 1,10-phen and tetramethylethylenediamine (tmeda), utilizing the sensitivity of 1s3p X-ray emission spectroscopy (Kβ XES) to the oxidation and spin states of 3d transition-metal ions, in addition to Co L-edge X-ray absorption spectroscopy (L-edge XAS) and ligand-field atomic-multiplet calculations of the Kβ XES and L-edge XAS spectra to confirm the LS-Co^{III} and HS-Co^{II} nature of the respective low and high temperature tautomers.[119] This study also suggested the possibility of hard X-rays inducing the VT interconversion. It has previously been established that soft X-rays can also induce VT in cobalt–dioxolene compounds.[120] Very shortly after the XAS study, Pinheiro and coworkers reported the first definitive evidence for a VT interconversion in the classic compound [Co(3,5-dbdiox)(3,5-dbSQ)(4-CNpy)$_2$]·benzene induced by synchrotron hard X-rays at temperatures below 60 K and monitored by single-crystal X-ray diffraction.[121] Attenuation of the X-ray beam decreases the fraction of interconversion.

The combination of ^{1}H and ^{59}Co nuclear and muon spin-lattice relaxation rate measurements has allowed investigation of the spin dynamics of photoinduced [Co^{II}(3,5-dbSQ)(Me_2tpa)]$^+$ in the solid state as a function of the temperature.[118] The lifetime of several hours below 30 K, is characterized by spin dynamics in the MHz range, which persist at least down to 10 K. These results imply that these species may not be suitable as logic units.

In another recent study focused on the dynamics of photo-induced VT, Vura-Weis, and coworkers employed $M_{2,3}$-edge X-ray absorption near-edge structure spectroscopy with 40 fs time resolution to probe photo-induced VT in a thick film of the VT compound [Co^{III}(Cat-N-SQ)(Cat-N-BQ)]/[Co^{II}(Cat-N-BQ)] produced by vacuum sublimation.[41] Femtosecond extreme UV transient absorption spectroscopy shows that 525 nm excitation of [Co^{III}(Cat-N-SQ)(Cat-N-BQ)] forms a LS-Co^{II} LMCT state within the 40 fs instrument response (Figure 15).[122] The complex then undergoes rapid intersystem crossing in 67 fs to a hot HS-Co^{II} state. Vibrational cooling in 460 fs competes with rapid back-intersystem crossing. The cold HS-Co^{II} state relaxes the ground state in 24 ps, depending on sample temperature and environment. This study has provided unprecedented access to the dynamics of photo-induced VT, revealing just how fast the relevant transitions are.

Encyclopedia of Inorganic and Bioinorganic Chemistry, Online © 2011–2021 John Wiley & Sons, Ltd.
This article is © 2021 John Wiley & Sons, Ltd.
This article was published in the *Encyclopedia of Inorganic and Bioinorganic Chemistry* in 2021 by John Wiley & Sons, Ltd.
DOI: 10.1002/9781119951438.eibc2785

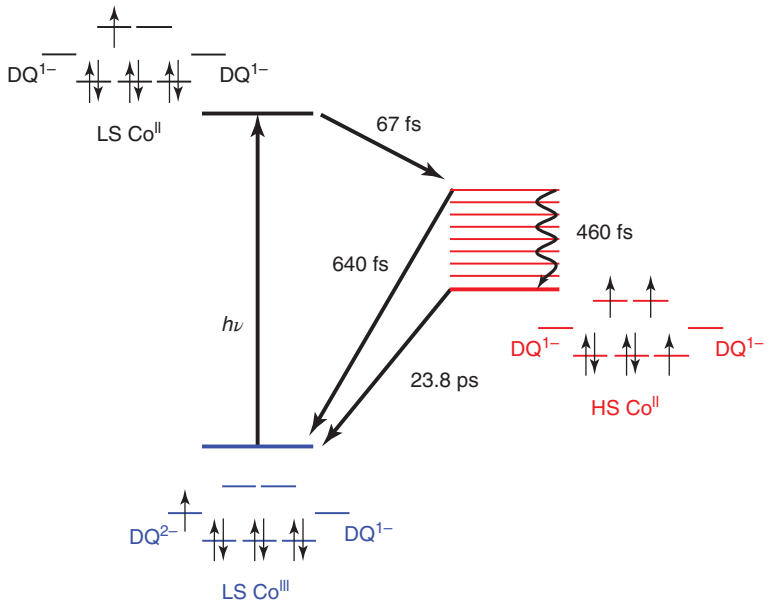

Figure 15 Proposed dynamics of photo-induced VT in a $[Co^{III}(Cat\text{-}N\text{-}SQ)(Cat\text{-}N\text{-}BQ)]/[Co^{II}(Cat\text{-}N\text{-}BQ)_2]$ thick film; (DQ = Cat-N-SQ and Cat-N-BQ). [Ash *et al.*[122]]

4 COMPUTATIONAL ADVANCES IN VALENCE TAUTOMERISM

4.1 Density Functional Theory for Valence Tautomerism

DFT is a computational chemistry methodology based on the understanding that all ground-state properties are completely determined by the electron density; however, the exact functional that describes how the ground state energy relates to the electron density is unknown. An error in DFT comes about because the different approximations to the exact form of the exchange-correlation part of the functional have varying degrees of accuracy.[36] The most basic DFT calculation is a single-point calculation of the energy; a geometry optimization can also be performed by iteratively adjusting the nuclear coordinates and calculating the resulting energy until both the coordinates and energy converge. Other contributions to the energy may be included to improve the accuracy of a DFT calculation such as zero-point energy (ZPE) corrections, relativistic corrections, dispersion forces, and solvent effects.[123] Solvent interactions can be included using the polarizable continuum model (PCM) or conductor-like screening model (COSMO), which can be used to obtain accurate geometries of metal complexes that include mixed anionic and neutral ligands.[124] Dispersion forces have been shown to be important to obtain accurate geometries and energies[36] and have been applied to SCO complexes but reports on VT complexes are limited.[73,125–129]

Spin and electronic transitions such as SCO and VT may be modeled with DFT by calculating the electronic energy difference between different electromeric forms, which is equal to the enthalpy change at 0 K, ΔH_{VT}.[130] The valence tautomers may be identified by bond length and spin density analysis, as popular DFT functionals give poor correlation between the atomic charges and formal oxidation states.[126] Vibrational analysis allows the enthalpy to be corrected to include the ZPE and gives ΔS_{vib} for the transition. The total entropy term ($\Delta S_{VT} = \Delta S_{vib} + R\ln(2S_f + 1) - R\ln(2S_i + 1)$, $S_{f/i}$ = total spin of final/initial state) can be used to simulate the molar fractions of each species with temperature and to find $T_{1/2}$; however, these values are often inaccurate as detailed below.

The main issue with using DFT for modeling transitions that involve a change in total spin is that DFT functionals are optimized to give good reproduction of thermochemical parameters and struggle to reproduce relative spin-state energies, which are highly sensitive to the exchange and correlation functionals used.[130] Generalized gradient approximation (GGA) functionals may give accurate results through cancellation of errors. For SCO and VT, the most successful GGA functional is OPBE, which can accurately reproduce energy gaps in Fe^{II} and Fe^{III} SCO complexes.[131,132] The OPBE functional can reproduce accurate ΔH_{VT} values but suggests that the experimentally unobserved LS-Co^{II}-$(SQ)_2$ state is lower in energy than the HS-Co^{II}-$(SQ)_2$ state for calculations of [Co(3,5-dbdiox)(3,5-dbSQ)(bpy)] (*t*-Bu replaced by H) and

Encyclopedia of Inorganic and Bioinorganic Chemistry, Online © 2011–2021 John Wiley & Sons, Ltd.
This article is © 2021 John Wiley & Sons, Ltd.
This article was published in the *Encyclopedia of Inorganic and Bioinorganic Chemistry* in 2021 by John Wiley & Sons, Ltd.
DOI: 10.1002/9781119951438.eibc2785

trans-[Co(3,5-dbdiox)(3,5-dbSQ)(4-papy)$_2$] (*t*-Bu replaced by Me).[52,133]

In general, GGAs underestimate the exchange contribution, affording an artificially high energy for the HS state.[130] The bias can be partially corrected for by incorporating a component of Hartree–Fock (HF) exchange. The popular hybrid functional, B3LYP has 20% HF exchange, tends to over-stabilize the HS state, and is not the functional of choice for cobalt VT. However, it correctly identifies the ground state tautomer in selected Fe, Cu, and Os VT complexes.[69,73,74] The reparametrized hybrid functional B3LYP* (15% HF exchange) has found success in a wide range of VT and SCO complexes[125]; it gives the correct ordering of electromers for [Co(3,5-dbdiox)(3,5-dbSQ)(bpy)],[133] and has been extensively used in studies on cobalt valence tautomers by Minkin, Starikov, and Starikova.[126,134] In complexes where the B3LYP* functional predicts the wrong ordering, the meta-hybrid TPSSh (10% HF exchange) can be used for more accurate results. Basis sets can also be extended, and diffuse and polarization functions included on all atoms to improve accuracy, such as the Pople 6-311++G(d,p) or Ahlrichs valence triple-zeta with polarization (def2-TZVP) basis sets.[126] The meta-hybrid, TPSSh, also gives accurate SCO enthalpies over a range of first-row transition metals and oxidation states.[123] While double hybrid functionals have been used for SCO complexes, they are yet to be applied to VT.[125,132]

As yet there is not one universally correct functional for spin-state changes. However, as functional-dependent biases are consistent within families of related complexes, as long as accurate energetics are known for one transition metal complex, spin-state energies can be predicted for similar complexes. It remains ever important to validate DFT methods by their ability to reproduce experimental data on the target compound, or structurally related compounds.[126]

The above method can describe VT transitions in gas phase and solution but does not describe VT in the crystalline phase. In SCO complexes, this has been addressed by periodic DFT calculations introducing an additional Hubbard exchange term, U.[135] The DFT + U method gives accurate $T_{1/2}$ for SCO complexes and can be combined with dispersion-corrected functionals.[136] The drawback in the DFT + U approach is the difficulty in parametrizing the U term, and it has not yet been applied to VT complexes.

Variable-temperature UV–Vis–NIR and IR spectra are used as evidence of VT equilibria, and DFT can help identify the species present and assign the observed transitions. Infrared spectra are generated by optimization and vibrational analysis in the harmonic approximation, while UV–Vis–NIR spectra are generated using time-dependent (TD)-DFT to calculate vertical spin-allowed electronic transitions. The resulting stick spectra are convoluted with Gaussian or Lorentzian functions. The B3LYP functional has been most widely used for IR and TD-DFT calculations and the energy of transitions are often scaled to match experiment—typically by 0.97–1 for IR spectra and as much as 0.90 for TD-DFT.[91,129] Tourón Toceda *et al*. and Azzaroli *et al*. used DFT to assign IR markers for cat^{2-}/ SQ$^{\bullet-}$ (B3LYP/Pople 6-31 + G(d,p)/gas phase) and Cat-N-SQ$^{\bullet 2-}$/Cat-N-BQ^{-} (B3LYP/Pople 6-31G(d,p)/gas phase) redox states, respectively, to identify the species present in the time-resolved IR study of light-induced VT.[137,138] Calculation of IR and UV–Vis spectra of the two valence tautomers of [Co(phendiox)(*rac*-cth)]$^{+}$ confirmed the species involved in the variable-temperature VT equilibrium in solution, and that light-irradiation at low temperature traps the metastable HS-Co^{II}-SQ form (B3LYP/Watchers-Hay (14s9p5d)/[9s5p3d]+f for Co, Pople 6-311 + G(d,p) for other atoms/COSMO).[91] A TD-DFT study of [Cu(L$_3$)$_2$]$^{+}$ was used to elucidate the equilibria between two tautomers observed in variable temperature and variable solvent UV–Vis–NIR spectra (B3LYP/SVP on C and H, TZVP on other atoms/conductor-like PCM).[73] TD-DFT can also be used to assign bands in the UV–Vis-NIR absorption spectrum of valence tautomers,[69,74] which has allowed determination of the charge transfer process that initiates the light-induced VT transition.[90]

There are other considerations when performing calculations on molecules with potential open-shell metals and radical ligands; the obtained wavefunctions should always be checked for stability.[129] The exchange interaction between metal and radical ligand (or multiple radical ligands) can be calculated according to the broken symmetry approximation. However, the broken symmetry approach is invalidated if the states have significant multi-reference character, which may occur for some radicals and metals with unquenched first-order orbital angular momentum (including octahedral HS-Co^{II}).[65,91] DFT can distinguish between true VT, where there are two electromers each with distinct metal and ligand oxidation states and geometries, and a single geometric minima that has features from multiple resonance structures.[139] Here, the HS and broken symmetry[65] solution have equivalent geometries and indistinguishable oxidation states.

4.2 Advances in Computational Prediction and Rationalization of Valence Tautomerism

The first DFT study of VT was reported by Noodleman, Hendrickson *et al*. in 1997 and focused on the complex [Co(3,5-dbdiox)(3,5-dbSQ)(1,10-phen)].[140] They studied the electronic structures, energy differences, approximate Co-SQ magnetic exchange interactions, and vertical optical transition energies for the LS-Co^{III}-(cat)(SQ), LS-Co^{II}-(SQ)$_2$, and HS-Co^{II}-(SQ)$_2$ electromers using GGA single point calculations on crystal structures modified to have hydrogen atoms in the place of *tert*-butyl groups (B86P86/DZP for Co, DZ for other atoms/gas phase). Metal–ligand covalent interactions were observed and

Encyclopedia of Inorganic and Bioinorganic Chemistry, Online © 2011–2021 John Wiley & Sons, Ltd.
This article is © 2021 John Wiley & Sons, Ltd.
This article was published in the *Encyclopedia of Inorganic and Bioinorganic Chemistry* in 2021 by John Wiley & Sons, Ltd.
DOI: 10.1002/9781119951438.eibc2785

the decreased $T_{1/2}$ for the title complex compared to the *N*,*N*,*N*′,*N*′-tmeda analog was attributed to increased π-backbonding. The calculations confirmed a LS-Co^{III}-(cat)(SQ) ground state but predicted the experimentally unobserved LS-Co^{II}-$(SQ)_2$ tautomer to be next lowest in energy.

Since 1997, developments in DFT methods and computer infrastructure have progressed to allow routine geometry optimizations, vibrational analysis, and calculation of transition states.[52,133] Minimum energy crossing points (MECPs) refer to the minimum energy in the nonadiabatic transition from one spin state to another and can be used to estimate barriers to spin interconversions. The MECPs, relative energies and relative entropy contributions can be used to determine which valence tautomer will participate in a VT equilibrium, including when there are multiple electromers with the same spin multiplicity.[126] For Yoshizawa and coworkers' calculations on [Co(3,5-dbdiox)(3,5-dbSQ)(bpy)], the MECPs indicate that thermally induced VT occurs in a single step between LS-Co^{III}-(cat)(SQ) and HS-Co^{II}-$(SQ)_2$ states, rather than via a LS-Co^{II}-$(SQ)_2$ intermediate (B3LYP*/Watchers-Hay (14s9p5d)/[9s5p3d]+f for Co, Pople 6-311G(d,p) for all other atoms/gas phase).[133] The DFT study of *trans*-[Co(3,5-dbdiox)(3,5-dbSQ)(4-papy)$_2$] was able to rationalize the observed experimental VT behavior (OPBE/SV(P) for C and H, TZV(P) for all other atoms/COSMO) and simulate the expected EPR and UV–Vis spectral evolution throughout the VT transition (B3LYP/CP(PPP) for Co, SVP-ZORA for C and H, TZV-ZORA for all other atoms/COSMO).[52] The relative energies of two valence tautomers were calculated for $[Cu(L_3)_2]^+$, optimized with the GGA functional BP86, B3LYP, or B3LYP with Grimme's D3 dispersion correction; the relative energies were functional-dependent but all methods correctly identified the ground state (various functionals/SVP for C and H, TZVP for all other atoms/conductor-like PCM).[73]

DFT can be used to understand structure-function correlations. An experimental study of 2-ferrocenyloxodihydrodibenzochromenylium salts by Kondo *et al*. indicated the dihedral angle between the ferrocene and the pyrylium moieties in the solid state correlated with the observed VT behavior, of lack thereof.[141] TD-DFT (B3LYP/Lanl2DZ/gas phase) revealed that a larger dihedral angle resulted in a larger HOMO–LUMO gap, presumably due to a weaker donor-acceptor interaction destabilizing the pyrylium-based LUMO, and disfavoring the iron(III) species at high temperature.

The group of Minkin, Starikov, and Starikova have extensively reported DFT calculations on cobalt valence tautomers, which they have reviewed recently.[126,134] These calculations have been performed for hypothetical neutral complexes with LS-Co^{III}-(L^{1-}) ⇆ HS-Co^{II}-(L^0) equilibria including semiquinone/benzoquinone ligands, iminosemiquinone/iminoquinone ligands, diimine ligands, imine substituted pyridine ligands, and analogous bis(bidentate) ligands in dinuclear compounds (B3LYP*/Pople 6-311++G(d,p)/gas phase). Numerous potential VT complexes have been identified in these studies but are yet to be confirmed experimentally. One essential part of these exploratory studies is to test the stability of the proposed complexes to dissociation, by using DFT to calculate the relative energy of the product complex relative to its dissociated products.

Recently, the same group has published calculations on the monocationic complexes $[Co(3,5\text{-dbdiox})(Me_n tpa)]^+$ (n = 0, 2, 3; *t*-Bu groups replaced by H).[142] Here, and in other complexes, inclusion of the counter ion was required to accurately reproduce the relative electromer energies with the TPSSh functional (TPSSh/Pople 6-311++G(d,p)/gas phase).[126] Subsequently, Boskovic and coworkers employed DFT calculations (OPBE/TZP-ZORA/COSMO) to screen various complexes of formula $[Co(diox)(Me_n tpa)]^+$ (n = 0–3; including diox = 3,5-dbdiox, Cl_4diox, Br_4diox) with the aim of identifying an appropriate method to allow accurate prediction of VT candidate compounds.[34] This approach was facilitated by the extensive experimental data available for the known VT complexes $[Co(3,5\text{-dbdiox})(Me_2tpa)]^+$ (Figure 3) and $[Co(Cl_4diox)(Me_3tpa)]^+$.[33,143] This work allowed the prediction of VT for the previously unreported $[Co(Br_4diox)(Me_3tpa)]^+$, which was subsequently synthesized and investigated experimentally to verify that it does indeed display thermally induced VT (Section 3.1.1). Another important point to come out of this work is that the often used time-saving substitution of *tert*-butyl groups for hydrogen atoms or methyl groups significantly affects the results and has the potential to lead to incorrect conclusions, particularly where the substituents are attached to redox-active ligands. Minkin and coworkers have observed that these simplification do not always make a difference, but are important if they affect the geometry of the complex.[126]

The related family of complexes [Co(AzaNR)(3,5-dbdiox)]$^+$ are of much interest as the R = *tert*-butyl analogue exhibits a thermally induced cobalt(II) SCO transition, the only cobalt–dioxolene complex known to do so.[64,129] In contrast, the R = isopropyl analog instead undergoes a thermal VT interconversion and the R = methyl and ethyl analogs are temperature independent LS-Co^{III}-cat up to 350 K.[57] DFT calculations (TPSSh/Pople 6-311++G(d,p)/gas phase) afforded energies for the different electromeric forms that are in excellent agreement with the experimental behavior (Figure 16).[57]

As discussed above (Section 3.2.1) dinuclear valence tautomeric complexes are of interest for the possibility of accessing a two-step VT transition. The earliest dinuclear complex of relevance to VT to be investigated

Encyclopedia of Inorganic and Bioinorganic Chemistry, Online © 2011–2021 John Wiley & Sons, Ltd.
This article is © 2021 John Wiley & Sons, Ltd.
This article was published in the *Encyclopedia of Inorganic and Bioinorganic Chemistry* in 2021 by John Wiley & Sons, Ltd.
DOI: 10.1002/9781119951438.eibc2785

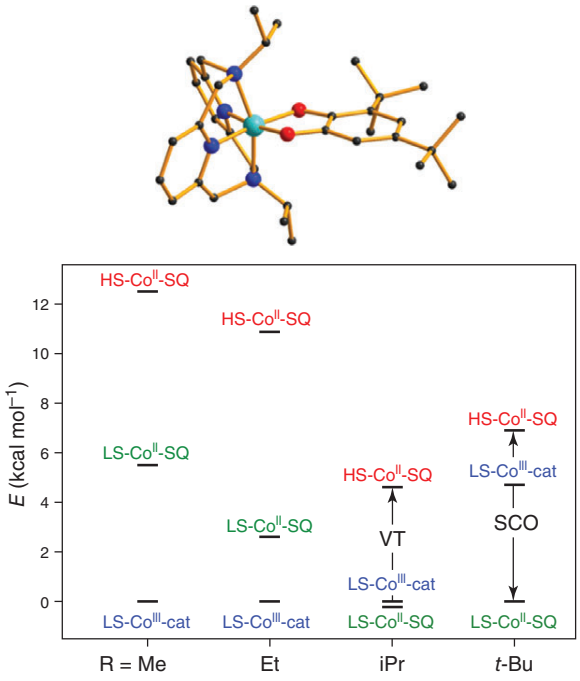

Figure 16 Structure of $[Co^{III}(AzaN\text{-}iPr)(3,5\text{-}dbcat)]^+$ and DFT (TPSSh/Pople 6-311++G(d,p)/gas phase) calculated energies for different electromeric forms of $[Co(AzaNR)(3,5\text{-}dbdiox)]^+$ (R = Me, Et, iPr and *t*-Bu). [Tezgerevska *et al.*[57]]

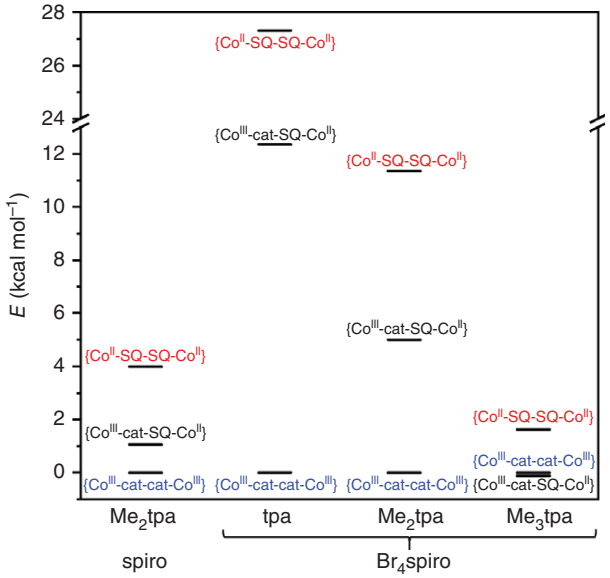

Figure 17 Density functional theory (TPSSh/Pople 6-311++G(d,p)/gas phase) calculated energies for different electromeric forms of dinuclear $[\{Co(Me_ntpa)\}_2(Xspiro)]^{2+}$ (Figure 7) with LS-Co^{III}-cat and HS-Co^{II}-SQ moieties. [Gransbury *et al.*[83]]

by DFT calculations was $[\{Co(cth)\}_2(diox\text{-}diox)](PF_6)$ in 2001 (diox-diox = 5,5′-di-*tert*-butyl-3,3′,4,4′-tetrahydroxybiphenyl) (PW91/DZP/gas phase).[144] In this work, the cth ligands were modeled as ammonia ligands and *tert*-butyl groups were modeled as methyl groups to reduce computational expense. The calculations were consistent with experimental data, indicating that the radical trianionic diox-diox ligand has full delocalization of the unpaired electron.

An important effort towards two-step transitions from the Boskovic group has involved investigation of the families of complexes $[\{Co(Me_ntpa)\}_2(Xspiro)]^{2+}$ (Figure 7).[83,84] DFT calculations (TPSSh/Pople 6-311++G(d,p)/gas phase) performed by A. Starikova have afforded key insights within this study. The experimental data indicate that the VT behavior depends critically on both the ancillary and bridging ligand, with no or incomplete VT observed for most analogs and only the $[\{Co(Me_2tpa)\}_2(spiro)]^{2+}$ complex exhibiting the desired two sequential one-electron steps at each cobalt–dioxolene unit. The relative energies of the three relevant electromeric forms (Figure 17) are key to achieving two-step VT and the DFT studies of the $[\{Co(Me_ntpa)\}_2(Xspiro)]^{2+}$ family indicate that only the $[\{Co(Me_2tpa)\}_2(spiro)]^{2+}$ complex has the appropriate ordering of energy levels, consistent with two-step VT being observed only for this species experimentally.

In a different vein, Droghetti and Sanvito employed single-point DFT calculations of $[Co(3,5\text{-}dbdiox)(Me_2tpa)]^+$ with Me_2tpa replaced with ammonia ligands (B3LYP/Pople 6-31G(d)/gas phase) to probe the effect of a static electric field on the thermal VT interconversion.[145] When the electric field is in the direction that facilitates VT electron transfer, the energy gap between tautomers decreases. Under the assumption that ΔS_{VT} is unchanged by the electric field, they predict that a field of 0.1 Vnm^{-1}, achievable in Stark spectroscopy experiments, could produce a change in the critical temperature for the interconversion of 20 K. In 2017, Klokishner and coworkers introduced an electric field into their microscopic model of a $[Co(diox)(SQ)(NL)_2]$ VT complex that includes parameters to describe electron transfer, crystal field splitting, magnetic exchange, vibronic coupling, and cooperative interactions.[146,147] The system was solved to obtain vibronic wavefunctions and energy levels, which are used to calculate the temperature-dependence of magnetic and optical properties. These results suggest that the VT transition temperature is dependent on the direction and intensity of the electric field. The possibility of tuning VT transition temperatures with an applied electric field is relevant for possible applications in electronic or spintronic devices but is yet to be confirmed experimentally.

Encyclopedia of Inorganic and Bioinorganic Chemistry, Online © 2011–2021 John Wiley & Sons, Ltd.
This article is © 2021 John Wiley & Sons, Ltd.
This article was published in the *Encyclopedia of Inorganic and Bioinorganic Chemistry* in 2021 by John Wiley & Sons, Ltd.
DOI: 10.1002/9781119951438.eibc2785

5 CONCLUDING REMARKS

The field of VT has come a long way since the first studies on [Co(3,5-dbdiox)(3,5-dbcat)(bpy)]. It is now known for metals across the d-block, as well as beyond, and with a wide variety of ligands. Various different stimuli have been found to induce VT including heating/cooling, photoirradiation, pressure, soft and hard X-rays, and intense magnetic fields. Moreover, a wide range of physical methods are useful for studying interconversions in the solid and solution states, in nano- and microparticles and in thin films and on surfaces.

A significant breakthrough in recent years is the demonstration of the utility of DFT calculations to provide important insights and guide synthetic efforts. The accuracy, computational cost, and reliability of modern DFT methods confer tremendous power on this approach. It is now clearly possible to a priori calculate previously unknown complexes and accurately predict the likelihood of VT. Moreover, it is possible to rationalize SCO versus VT and the stepwise or concerted nature of two-step interconversions. An important lesson is that the long-standing practice of replacing sterically bulky and computationally expensive functional groups with smaller ones can invalidate results and should be treated with caution.

An obvious comparison of VT is with its phenomenologically related, but much more extensively studied cousin, SCO. The method of tuning the characteristics of VT transitions is different, involving modulating both steric and electronic effects to effectively match the redox potentials of the metal and redox-active ligand, in contrast to the simpler tuning of ligand field that controls SCO. A wider range of metal and ligand systems can exhibit VT than SCO. In terms of colorimetric-based applications, VT can offer access to colors that are unavailable with SCO. Perhaps more importantly, the intramolecular electron transfer that is intrinsic to VT affords additional possibilities in terms of applications based on charge transport, conductivity, or macroscopic polarization.

Although yet to be realized practically, VT remains of considerable promise for chemical reactivity and catalysis. Its relevance to the function of a range of metalloenzymes in biology is a testament to this. An exciting future prospect is a thermally or photoswitchable catalyst, for example where distinct valence tautomeric forms can be interconverted and can then catalyze different chemical processes. Clearly, the future is bright for this field.

6 ABBREVIATIONS

1,10-phen = 1,10-phenanthroline; 3,5-dbdiox = 3,5-di-*tert*-butyldioxolene; 3,5-dbSQ$^{\bullet-}$ = 3,5-di-*tert*-butylsemiquinonate; 3,5-di-BrPy = 3,5-dibromopyridine; 3,5-di-ClPy = 3,5-dichloropyridine; 3,5-Me_2-BIAN = *N*,*N*′-bis(3,5-dimethylphenylimino)acenaphthylene; 3,6-dbdiox = 3,6-di-*tert*-butyldioxolene; 3,6-dbSQ$^{\bullet-}$ = 3,6-di-*tert*-butylsemiquinonate; 4,5-pip-3,6-dbdiox = 3,6-di-*tert*-butyl-4,5-*N*,*N*′-piperazino-*o*-benzoquinone; 4-Cl-3,6-dbdiox = 3,6-di-*tert*-butyl-4-Cl-*o*-benzoquinone; 4-CN-py = 4-cyanopyridine; 4-*N*-TEMPO-ip = [2,2,6,6-tetramethyl-4-[[(*E*)-pyridin-2-ylmethylidene]amino]*cyclo*-hexyl]oxidanyl; 4-NO_2-py = 4-nitropyridine; 4-OMe-3,6-dbdiox = 4-methoxy-3,6-di-*tert*-butyl-dioxolene; 4-papy = 4-phenylazopyridine; 4-stypy = 4-styrylpyridine; An-BODIPY-diox = 9-(3,4-dihydroxyphenyl)-10-[4,4-difluoro-1,3,5,7-tetramethyl-8-(phenyl)-4-bora-3a,4a-diaza-*s*-indacene]anthracene; An diox = 9-(3,4-di-hydroxyphenyl)anthracene; AP^{2-} = amidophenolate; APSO = 4-methylspiro[4-azahomoadamantane-5,2′-[2H-1,4]ox-azino-[2,3-f][1,10]phenanthroline; AzaNR = *N*,*N*′-di-alkyl-2,11-diaza[3.3]-(2,6)pyridinophane; BIAN = bis(arylimino)acenapthene; bpi = bis(pyridylimino)isoindoline; bpqa = (bis(2-pyridylmethyl)(2-quinolylmethyl)amine; bpy = 2,2′-bipyridine; bpym = 2,2′-bipyrimidine; Br_3pycat^{2-} = 3,5,6-tribromo-4-pyridinium-catecholate; Br_4diox = tetrabromodioxolene; Br_4 spiroH_4 = 3,3,3′,3′-tetramethyl-1,1′-spirobi(indan)-4,4′,7,7′-tetrabromo-5,5′,6,6′-tetraol; $Br_4SQ^{\bullet-}$ = tetrabromosemiquinonate; cat^{2-} = catecholate; Cat-N-BQ^{-} = monanionic form of 3,5-di-*tert*-butyl-1,2-quinone-1-(2-hydroxy-3,5-di-*tert*-butylphenyl)-imine; Cat-N-$SQ^{\bullet 2-}$ = radical dianionic form of 3,5-di-*tert*-butyl-1,2-quinone-1-(2-hydroxy-3,5-di-*tert*-butylphenyl)-imine; Cl_2AnH_2 = chloranilic acid; COSMO = conductor-like solvent model; CP = coordination polymer; cth = 5,5,7,12,12,14-hexamethyl-1,4,8,11-tetraazacyclotetradecane; CTIST = charge transfer induced spin transition; dbdioxSH = 4,6-di-*tert*-butyl-3-((4-(mercaptomethyl)benzyl)thio)benzene-1,2-hydroxy-dioxolene; diox-diox = 5,5′-di-*tert*-butyl-3,3′,4,4′-tetrahydroxybiphenyl; DBE = 1,2-dibromoethane; DCE = 1,2-dichloroethane; DCM = dichloromethane; DFT = density functional theory; diox = *ortho*-dioxolene; dipyydH = 1-isopropyl-3,5-dipyridyl-6-oxoverdazyl; dhbq = 2,5-dihydroxy-1,4-benzoquinone; EPR = electron paramagnetic resonance; ETCST = electron transfer coupled spin transition; GGA = generalized gradient approximation; HF = Hartree-Fock; HOMO = highest occupied molecular orbital; HS = high spin; IBQ = iminobenzoquinone; ISQ$^{\bullet-}$ = iminobenzosemiquinonate; L_1H_2 = 2-(2-phenylazo)-anilino-4,6-di-*tert*-butylphenol; L_2 = 5,6-bis-(*N*,*N*′-dimethyl-*N*,*N*′-ethylene-guanidino)-2,2-dimethyl-[1,3]-benzodioxole; L_3H_2 = (2-[2-(benzylthio)phenyl-amino]-4,6-di-*tert*-butylphenol; L_4H_2 = *N*-(benzophenoxazine)-*o*-aminophenol; L_5 = 2,3,5,6-tetrakis(tetramethyl-guanidino)pyridine; $L_6^{\bullet-}$ = 3,6-bis(pyridyl)-1,2,4,5-tetrazine radical; L_7 = 3,3′,5,5′-tetrakis(4-pyridyl)bimesityl; LMCT = ligand to metal charge transfer; LS = low spin; LUMO = lowest unoccupied molecular orbital; MeCN = acetonitrile; MECP = minimum energy crossing point; Metpa = bis(2-pyri-

Encyclopedia of Inorganic and Bioinorganic Chemistry, Online © 2011–2021 John Wiley & Sons, Ltd.
This article is © 2021 John Wiley & Sons, Ltd.
This article was published in the *Encyclopedia of Inorganic and Bioinorganic Chemistry* in 2021 by John Wiley & Sons, Ltd.
DOI: 10.1002/9781119951438.eibc2785

dylmethyl)(6-methyl-2-pyridylmethyl)amine; Me_2tpa = bis(6-methyl-2-pyridylmethyl)(2-pyridylmethyl)amine; Me_3tpa = tris(6-methyl-2-pyridylmethyl)amine; MOF = metal-organic-framework; NIR = near infrared; NITImH = 2-(2-imidazolyl)-4,4,5,5-tetramethyl-4,5-dihydro-1H-3-oxide-1-oxyl); OMP = 2,2′-(pyridine-2,6-diyl)bis(N1,N1,N3,N3-tetramethylpropane-1,3-diamine; pbqa = (2-pyridylmethyl)bis(2-quinolylmethyl)amine; PCM = polarizable continuum model; phendioxH_2 = 9, 10-dihydroxyphenanthrene; PISCES = photoisomerization-induced spin−charge excited state; PMMA = poly(methyl methacrylate); py = pyridine; py_2O = bis(pyridyl)ether; SCO = spin crossover; spiroH_4 = 3,3,3′,3′-tetramethyl-1,1′-spirobis(indane)-5,5′,6,6′-tetrol; $SQ^{\bullet-}$ = semiquinonate; tmeda = tetramethylethylenediamine; tol = toluene; tpa = tris(2-pyridylmethyl)amine; tqa = tris(2-quinolylmethyl)amine; tpom = tetrakis(4-pyridyloxymethylene)methane; UV = ultraviolet; vis = visible; VT = valence tautomerism; XAS = X-ray emission spectroscopy; XES = X-ray emission spectroscopy; XPS = X-ray photoelectron spectroscopy

7 ACKNOWLEDGMENTS

We thank the Australian Research Council for funding our work in this field (DP190100854, DP150100353, DP110100155). We would like to thank all the other Boskovic group members who have participated in work on valence tautomerism over the years, especially Yanyan Mulyana, Kerwyn Alley, Olga Drath, and Tina Tezgerevska.

8 RELATED ARTICLES

Cobalt: Inorganic & Coordination Chemistry; Electron Transfer in Coordination Compounds; Iron: Inorganic & Coordination Chemistry; Manganese: Inorganic & Coordination Chemistry; Mixed Valence Compounds; Vanadium: Inorganic & Coordination Chemistry; Approximate Density Functionals: Which Should I Choose?; Metal-Organic Frameworks: Coordination Polymer Nanoparticles and Macrostructures; Charge Transfer; Density Functional Theory

9 REFERENCES

1. W. Kaim and B. Schwederski, *Coord. Chem. Rev.*, 2010, **254**, 1580.
2. W. Kaim, *Inorg. Chem.*, 2011, **50**, 9752.
3. O. R. Luca and R. H. Crabtree, *Chem. Soc. Rev.*, 2013, **42**, 1440.
4. J. I. van der Vlugt, *Chem. Eur. J.*, 2019, **25**, 2651.
5. K. S. Pedersen, P. Perlepe, M. L. Aubrey, D. N. Woodruff, S. E. Reyes-Lillo, A. Reinholdt, L. Voigt, Z. Li, K. Borup, M. Rouzières, D. Samohvalov, F. Wilhelm, A. Rogalev, J. B. Neaton, J. R. Long and R. Clérac, *Nat. Chem.*, 2018, **10**, 1056.
6. Y. Zhang, S. N. Riduan and J. Wang, *Chem. Eur. J.*, 2017, **23**, 16419.
7. J. Ferrando-Soria, J. Vallejo, M. Castellano, J. Martínez-Lillo, E. Pardo, J. Cano, I. Castro, F. Lloret, R. Ruiz-García and M. Julve, *Coord. Chem. Rev.*, 2017, **339**, 17.
8. K. Senthil Kumar and M. Ruben, *Coord. Chem. Rev.*, 2017, **346**, 176.
9. D. Aguila, Y. Prado, E. S. Koumousi and R. Clérac, *Chem. Soc. Rev.*, 2016, **45**, 203.
10. R. M. Metzger, *Chem. Rev.*, 2015, **115**, 5056.
11. E. Coronado, *Nat. Rev. Mater.*, 2020, **5**, 87.
12. T. Tezgerevska, K. G. Alley and C. Boskovic, *Coord. Chem. Rev.*, 2014, **268**, 23.
13. D. N. Hendrickson and C. G. Pierpont, *Top. Curr. Chem.*, 2004, **234**, 63.
14. A. Dei, D. Gatteschi, C. Sangregorio and L. Sorace, *Acc. Chem. Res.*, 2004, **37**, 827.
15. O. Sato, *J. Photochem. Photobiol. C Photochem. Rev.*, 2004, **5**, 203.
16. E. Evangelio and D. Ruiz-Molina, *Eur. J. Inorg. Chem.*, 2005, 2957.
17. O. Sato, A. Cui, R. Matsuda, J. Tao and S. Hayami, *Acc. Chem. Res.*, 2007, **40**, 361.
18. O. Sato, J. Tao and Y.-Z. Zhang, *Angew. Chem. Int. Ed. Eng.*, 2007, **46**, 2152.
19. E. Evangelio and D. Ruiz-Molina, *Comptes Rendus Chim.*, 2008, **11**, 1137.
20. A. Dei and L. Sorace, *Appl. Magn. Reson.*, 2010, **38**, 139.
21. C. Boskovic, in 'Spin-Crossover Materials Properties and Applications', ed. M. A. Halcrow, John Wiley & Sons, Chichester, 2013, p. 203.
22. H.-C. Chang and D. Kiriya, *Eur. J. Inorg. Chem.*, 2013, 642.
23. O. Sato, *Nat. Chem.*, 2016, **8**, 644.
24. N. A. Váquez-Mera, F. Novio, C. Roscini, C. Bellacanzone, M. Guardingo, J. Hernando and D. Ruiz-Molina, *J. Mater. Chem. C*, 2016, **4**, 5879.
25. O. Drath and C. Boskovic, *Coord. Chem. Rev.*, 2018, **375**, 256.
26. A. Rajput, A. K. Sharma, S. K. Barman, A. Saha and R. Mukherjee, *Coord. Chem. Rev.*, 2020, **414**, 213240.
27. H. J. Himmel, *Inorg. Chim. Acta*, 2018, **481**, 56.

Encyclopedia of Inorganic and Bioinorganic Chemistry, Online © 2011–2021 John Wiley & Sons, Ltd.
This article is © 2021 John Wiley & Sons, Ltd.
This article was published in the *Encyclopedia of Inorganic and Bioinorganic Chemistry* in 2021 by John Wiley & Sons, Ltd.
DOI: 10.1002/9781119951438.eibc2785

28. M. Wang, Z.-Y. Li, R. Ishikawa and M. Yamashita, *Coord. Chem. Rev.*, 2021, **435**, 213819.
29. R. M. Buchanan and C. G. Pierpont, *J. Am. Chem. Soc.*, 1980, **102**, 4951.
30. D. M. Adams and D. N. Hendrickson, *J. Am. Chem. Soc.*, 1996, **118**, 11515.
31. O. Sato, S. Hayami, Z. Gu, K. Seki, R. Nakajima and A. Fujishima, *Chem. Lett.*, 2001, **30**, 874.
32. O. Sato, S. Hayami, Z. Gu, K. Takahashi, R. Nakajima and A. Fujishima, *Chem. Phys. Lett.*, 2002, **355**, 169.
33. A. Beni, A. Dei, S. Laschi, M. Rizzitano and L. Sorace, *Chem. Eur. J.*, 2008, **14**, 1804.
34. G. K. Gransbury, M.-E. Boulon, S. Petrie, R. W. Gable, R. J. Mulder, L. Sorace, R. Stranger and C. Boskovic, *Inorg. Chem.*, 2019, **58**, 4230.
35. D. M. Adams, A. Dei, A. L. Rheingold and D. N. Hendrickson, *Angew. Chem. Int. Ed.*, 1993, **32**, 880.
36. V. L. Nadurata and C. Boskovic, *Inorg. Chem. Front.*, 2021, **8**, 1840.
37. A. Bencini, A. Caneschi, C. Carboner, A. Dei, D. Gatteschi, R. Righini, C. Sangregorio and J. Van Slageren, *J. Mol. Struct.*, 2003, **656**, 141.
38. O.-S. Jung, D. H. Jo, Y.-A. Lee, B. J. Conklin and C. G. Pierpont, *Inorg. Chem.*, 1997, **36**, 19.
39. P. Dapporto, A. Dei, G. Poneti and L. Sorace, *Chem. Eur. J.*, 2008, **14**, 10915.
40. Y. Mulyana, G. Poneti, B. Moubaraki, K. S. Murray, B. F. Abrahams, L. Sorace and C. Boskovic, *Dalton Trans.*, 2010, **39**, 4757.
41. E. Evangelio, M.-L. Bonnet, M. Cabañas, M. Nakano, J.-P. Sutter, A. Dei, V. Robert and D. Ruiz-Molina, *Chem. Eur. J.*, 2010, **16**, 6666.
42. N. Shaikh, S. Goswami, A. Panja, X.-Y. Wang, S. Gao, R. J. Butcher and P. Banerjee, *Inorg. Chem.*, 2004, **43**, 5908.
43. D. Ruiz-Molina, K. Wurst, D. N. Hendrickson, C. Rovira and J. Veciana, *Adv. Funct. Mater.*, 2002, **12**, 347.
44. J. Guasch, L. Grisanti, S. Jung, D. Morales, G. D'Avino, M. Souto, X. Fontrodona, A. Painelli, F. Renz, I. Ratera and J. Veciana, *Chem. Mater.*, 2013, **25**, 808.
45. J. Rall, M. Wanner, M. Albrecht, F. M. Hornung and W. Kaim, *Chem. Eur. J.*, 1999, **5**, 2802.
46. H. Ohtsu and K. Tanaka, *Chem. Eur. J.*, 2005, **11**, 3420.
47. I. Ando, T. Fukuishi, K. Ujimoto and H. Kurihara, *Inorg. Chim. Acta*, 2012, **390**, 47.
48. N. Kundu, M. Maity, P. B. Chatterjee, S. J. Teat, A. Endo and M. Chaudhury, *J. Am. Chem. Soc.*, 2011, **1**, 20104.
49. T. Glaser, M. Heidemeier, R. Fröhlich, P. Hildebrandt, E. Bothe and E. Bill, *Inorg. Chem.*, 2005, **44**, 5467.
50. A. Panja, N. C. Jana, A. Bauzá, A. Frontera and C. Mathonière, *Inorg. Chem.*, 2016, **55**, 8331.
51. V. R. Hathwar, M. Stingaciu, B. Richter, J. Overgaard and B. B. Iversen, *Acta Cryst.*, 2017, **B73**, 304.
52. A. Witt, F. W. Heinemann, S. Sproules and M. M. Khusniyarov, *Chem. Eur. J.*, 2014, **20**, 11149.
53. A. Witt, F. W. Heinemann and M. M. Khusniyarov, *Chem. Sci.*, 2015, **6**, 4599.
54. M. A. Ribeiro, D. E. Stasiw, P. Pattison, P. R. Raithby, D. A. Shultz and C. B. Pinheiro, *Cryst. Growth Des.*, 2016, **16**, 2385.
55. M. Slota, M. Blankenhorn, E. Heintze, M. Vu, R. Hübner and L. Bogani, *Faraday Discuss.*, 2015, **185**, 347.
56. M. Bubnov, N. Skorodumova, A. Arapova, N. Smirnova, A. Bogomyakov, M. Samsonov, V. Cherkasov and G. Abakumov, *Polyhedron*, 2015, **85**, 165.
57. T. Tezgerevska, E. Rousset, R. W. Gable, G. N. L. Jameson, E. C. Sañudo, A. Starikova and C. Boskovic, *Dalton Trans.*, 2019, **48**, 11674.
58. T. Mibu, Y. Suenaga, T. Okubo, M. Maekawa and T. Kuroda-Sowa, *Inorg. Chem. Commun.*, 2020, **114**, 107826.
59. K. Katayama, M. Hirotsu, I. Kinoshita and Y. Teki, *Dalton Trans.*, 2014, **43**, 13384.
60. A. Panja and A. Frontera, *Eur. J. Inorg. Chem.*, 2018, **7**, 924.
61. R. D. Schmidt, D. A. Shultz, J. D. Martin and P. D. Boyle, *J. Am. Chem. Soc.*, 2010, **132**, 6261.
62. A. A. Zolotukhin, M. P. Bubnov, A. V. Arapova, G. K. Fukin, R. V. Rumyantcev, A. S. Bogomyakov, A. V. Knyazev and V. K. Cherkasov, *Inorg. Chem.*, 2017, **56**, 14751.
63. M. P. Bubnov, K. A. Kozhanov, N. A. Skorodumova and V. K. Cherkasov, *Inorg. Chem.*, 2020, **59**, 6679.
64. M. Graf, G. Wolmershäuser, H. Kelm, S. Demeschko, F. Meyer and H.-J. Krüger, *Angew. Chem. Int. Ed.*, 2010, **49**, 950.
65. G. K. Gransbury, M.-E. Boulon, R. A. Mole, R. W. Gable, B. Moubaraki, K. S. Murray, L. Sorace, A. Soncini and C. Boskovic, *Chem. Sci.*, 2019, **10**, 8855.
66. C. Fleming, D. Chung, S. Ponce, D. J. R. Brook, J. DaRos, R. Das, A. Ozarowski and S. A. Stoian, *Chem. Commun.*, 2020, **56**, 4400.
67. J. Bendix and K. M. Clark, *Angew. Chem. Int. Ed.*, 2016, **55**, 2748.
68. A. Panja, N. Ch. Jana, M. Patra, P. Brandão, C. E. Moore, D. M. Eichhorn and A. Frontera, *J. Mol. Catal.*, 2016, **A412**, 56.
69. A. Rajput, A. K. Sharma, S. K. Barman, D. Koley, M. Steinert and R. Mukherjee, *Inorg. Chem.*, 2014, **53**, 36.
70. A. Scheja, D. Baabe, D. Menzel, C. Pietzonka, P. Schweyen and M. Bröring, *Chem. Eur. J.*, 2015, **21**, 14196.
71. P. K. Das, S. Samanta, A. B. McQuarters, N. Lehnert and A. Dey, *Proc. Natl. Acad. Sci. USA*, 2016, **113**, 6611.
72. D. F. Schrempp, E. Kaifer, H. Wadepohl and H.-J. Himmel, *Chem. Eur. J.*, 2016, **22**, 16187.

Encyclopedia of Inorganic and Bioinorganic Chemistry, Online © 2011–2021 John Wiley & Sons, Ltd.
This article is © 2021 John Wiley & Sons, Ltd.
This article was published in the *Encyclopedia of Inorganic and Bioinorganic Chemistry* in 2021 by John Wiley & Sons, Ltd.
DOI: 10.1002/9781119951438.eibc2785

73. A. Rajput, A. Saha, S. K. Barman, F. Lloret and R. Mukherjee, *Dalton Trans.*, 2019, **48**, 1795.
74. S. Mondal, S. Bera, S. Maity and P. Ghosh, *ACS Omega*, 2018, **3**, 13323.
75. J. Cirera and E. Ruiz, *J. Mater. Chem. C*, 2015, **3**, 7954.
76. J.-A. Real, H. Bolvin, A. Bousseksou, A. Dworkin, O. Kahn, F. Varret and J. Zarembowitch, *J. Am. Chem. Soc.*, 1992, **114**, 4650.
77. S. Zein and S. A. Borshch, *J. Am. Chem. Soc.*, 2005, **127**, 16197.
78. J. Tao, H. Maruyama and O. Sato, *J. Am. Chem. Soc.*, 2006, **128**, 1790.
79. G.-L. Li, S. Kanegawa, Z.-S. Yao, S.-Q. Su, S.-Q. Wu, Y.-G. Huang, S. Kang and O. Sato, *Chem. Eur. J.*, 2016, **22**, 17130.
80. F. Yu, M. Xiang, Q.-G. Wu, H. He, S.-Q. Cheng, X.-Y. Cai, A.-H. Li, Y.-M. Zhang and B. Li, *Inorg. Chim. Acta*, 2015, **426**, 146.
81. N. Ch. Jana, P. Brandão, C. Mathonière and A. Panja, *Polyhedron*, 2018, **144**, 152.
82. D. Schweinfurth, Y. Rechkemmer, S. Hohloch, N. Deibel, I. Peremykin, J. Fiedler, R. Marx, P. Neugebauer, J. van Slageren and B. Sarkar, *Chem. Eur. J.*, 2014, **20**, 3475.
83. G. K. Gransbury, B. N. Livesay, J. T. Janetzki, M. A. Hay, R. W. Gable, M. P. Shores, A. Starikova and C. Boskovic, *J. Am. Chem. Soc.*, 2020, **142**, 10692.
84. K. G. Alley, G. Poneti, P. S. D. Robinson, A. Nafady, B. Moubaraki, J. B. Aitken, S. C. Drew, C. Ritchie, B. F. Abrahams, R. K. Hocking, K. S. Murray, A. M. Bond, H. H. Harris, L. Sorace and C. Boskovic, *J. Am. Chem. Soc.*, 2013, **135**, 8304.
85. M. P. Bubnov, N. A. Skorodumova, A. A. Zolotukhin, A. V. Arapova, E. V. Baranov, A. Stritt, A. Ünal, A. Grohmann, F. W. Heinemann, A. S. Bogomyakov, N. N. Smirnova, V. K. Cherkasov and G. A. Abakumov, *Z. Anorg. Allg. Chem.*, 2014, **640**, 2177.
86. S. Wiesner, A. Wagner, E. Kaifer and H.-J. Himmel, *Chem. Eur. J.*, 2016, **22**, 10438.
87. B. Li, X.-N. Wang, A. Kirchon, J.-S. Qin, J.-D. Pang, G.-L. Zhuang and H.-C. Zhou, *J. Am. Chem. Soc.*, 2018, **140**, 14581.
88. K. Katayama, M. Hirotsu, A. Ito and Y. Teki, *Dalton Trans.*, 2016, **45**, 10165.
89. M. M. Paquette, D. Plaul, A. Kurimoto, B. O. Patrick and N. L. Frank, *J. Am. Chem. Soc.*, 2018, **140**, 14990.
90. S. Kanegawa, Y. Shiota, S. Kang, K. Takahashi, H. Okajima, A. Sakamoto, T. Iwata, H. Kandori, K. Yoshizawa and O. Sato, *J. Am. Chem. Soc.*, 2016, **138**, 14170.
91. S.-Q. Wu, M. Liu, K. Gao, S. Kanegawa, Y. Horie, G. Aoyama, H. Okajima, A. Sakamoto, M. L. Baker, M. S. Huzan, P. Bencok, T. Abe, Y. Shiota, K. Yoshizawa, W. Xu, H.-Z. Kou and O. Sato, *Nat. Commun.*, 2020, **11**, 5.
92. O.-S. Jung and C. G. Pierpont, *J. Am. Chem. Soc.*, 1994, **116**, 2229.
93. I. Imaz, D. Maspoch, C. Rodríguez-Blanco, J. M. Pérez-Falcón, J. Campo and D. Ruiz-Molina, *Angew. Chem. Int. Ed.*, 2008, **47**, 1857.
94. L.-Q. Chen, R.-J. Wei, J. Tao, R.-B. Huang and L.-S. Zheng, *Sci. China Chem.*, 2012, **55**, 1037.
95. X.-Y. Chen, R.-J. Wei, L.-S. Zheng and J. Tao, *Inorg. Chem.*, 2014, **53**, 13212.
96. O. Drath, R. W. Gable, B. Moubaraki, K. S. Murray, G. Poneti, L. Sorace and C. Boskovic, *Inorg. Chem.*, 2016, **55**, 4141.
97. O. Drath, R. W. Gable, G. Poneti, L. Sorace and C. Boskovic, *Cryst. Growth Des.*, 2017, **17**, 3156.
98. W.-Q. Cheng, G.-L. Li, R. Zhang, Z.-H. Ni, W.-F. Wang and O. Sato, *J. Mol. Struct.*, 2015, **1087**, 68.
99. M. Guardingo, F. Busqué, F. Novio and D. Ruiz-Molina, *Inorg. Chem.*, 2015, **54**, 6776.
100. B. Li, L.-Q. Chen, R.-J. Wei, J. Tao, R.-B. Huang, L.-S. Zheng and Z. Zheng, *Inorg. Chem.*, 2011, **50**, 424.
101. A. Lannes, Y. Suffren, J. B. Tommasino, R. Chiriac, F. Toche, L. Khrouz, F. Molton, C. Duboc, I. Kieffer, J.-L. Hazemann, C. Reber, A. Hauser and D. Luneau, *J. Am. Chem. Soc.*, 2016, **138**, 16493.
102. C. Lecourt, Y. Izumi, L. Khrouz, F. Toche, R. Chiriac, N. Bélanger-Desmarais, C. Reber, O. Fabelo, K. Inoue, C. Desroches and D. Luneau, *Dalton Trans.*, 2020, **49**, 15646.
103. C. Lecourt, Y. Izumi, K. Maryunina, K. Inoue, N. Bélanger-Desmarais, C. Reber, C. Desroches and D. Luneau, *Chem. Commun.*, 2021, **57**, 2376.
104. J. Chen, Y. Sekine, Y. Komatsumaru, S. Hayami and H. Miyasaka, *Angew. Chem. Int. Ed.*, 2018, **57**, 12043.
105. B. Li, Y.-M. Zhao, A. Kirchon, J.-D. Pang, X.-Y. Yang, G.-L. Zhuang and H.-C. Zhou, *J. Am. Chem. Soc.*, 2019, **141**, 6822.
106. L. Amorín-Ferré, F. Busqué, J. L. Bourdelande, D. Ruiz-Molina, J. Hernando and F. Novio, *Chem. Eur. J.*, 2013, **19**, 17508.
107. F. Novio and D. Ruiz-Molina, *RSC Adv.*, 2014, **4**, 15293.
108. F. Nador, F. Novio and D. Ruiz-Molina, *Chem. Commun.*, 2014, **50**, 14570.
109. N. A. Vázquez-Mera, C. Roscini, J. Hernando and D. Ruiz-Molina, *Adv. Funct. Mater.*, 2015, **25**, 4129.
110. F. Novio, E. Evangelio, N. Vazquez-Mera, P. González-Monje, E. Bellido, S. Mendes, N. Kehagias and D. Ruiz-Molina, *Sci. Rep.*, 2013, **3**, 1.
111. S. Bin-Salamon, S. Brewer, S. Franzen, D. L. Feldheim, S. Lappi and D. A. Shultz, *J. Am. Chem. Soc.*, 2005, **127**, 5328.

Encyclopedia of Inorganic and Bioinorganic Chemistry, Online © 2011–2021 John Wiley & Sons, Ltd.
This article is © 2021 John Wiley & Sons, Ltd.
This article was published in the *Encyclopedia of Inorganic and Bioinorganic Chemistry* in 2021 by John Wiley & Sons, Ltd.
DOI: 10.1002/9781119951438.eibc2785

112. G. Poneti, L. Poggini, M. Mannini, B. Cortigiani, L. Sorace, E. Otero, P. Sainctavit, A. Magnani, R. Sessoli and A. Dei, *Chem. Sci.*, 2015, **6**, 2268.
113. P. González-Monje, F. Novio and D. Ruiz-Molina, *Chem. Eur. J.*, 2015, **21**, 10094.
114. M. Guardingo, P. González-Monje, F. Novio, E. Bellido, F. Busqué, G. Molnár, A. Bousseksou and D. Ruiz-Molina, *ACS Nano*, 2016, **10**, 3206.
115. C. Roux, D. M. Adams, J. P. Itié, A. Polian, D. N. Hendrickson and M. Verdaguer, *Inorg. Chem.*, 1996, **35**, 2846.
116. A. Caneschi, A. Dei, F. Fabrizi de Biani, P. Gütlich, V. Ksenofontov, G. Levchenko, A. Hoefer and F. Renz, *Chem. Eur. J.*, 2001, **7**, 3926.
117. B. Li, F.-L. Yang, J. Tao, O. Sato, R.-B. Huang and L.-S. Zheng, *Chem. Commun.*, 2008, 6019.
118. F. Caracciolo, M. Mannini, G. Poneti, M. Pregelj, N. Janša, D. Arčon and P. Carretta, *Phys. Rev. B*, 2018, **98**, 054416.
119. H. W. Liang, T. Kroll, D. Nordlund, T.-C. Weng, D. Sokaras, C. G. Pierpont and K. J. Gaffney, *Inorg. Chem.*, 2017, **56**, 737.
120. G. Poneti, M. Mannini, L. Sorace, P. Sainctavit, M.-A. Arrio, E. Otero, J. C. Cezar and A. Dei, *Angew. Chem. Int. Ed.*, 2010, **49**, 1954.
121. T. M. Francisco, W. J. Gee, H. J. Shepherd, M. R. Warren, D. A. Shultz, P. R. Raithby and C. B. Pinheiro, *J. Phys. Chem. Lett.*, 2017, **8**, 4774.
122. R. Ash, K. Zhang and J. Vura-Weis, *J. Chem. Phys.*, 2019, **151**, 104201.
123. J. Cirera, M. Via-Nadal and E. Ruiz, *Inorg. Chem.*, 2018, **57**, 14097.
124. R. K. Hocking, R. J. Deeth and T. W. Hambley, *Inorg. Chem.*, 2007, **46**, 8238.
125. K. P. Kepp, *Inorg. Chem.*, 2016, **55**, 2717.
126. V. I. Minkin, A. G. Starikov and A. A. Starikova, *Pure Appl. Chem.*, 2018, **90**, 811.
127. D. Manna, R. Lo and P. Hobza, *Dalton Trans.*, 2020, **49**, 164.
128. A. Miyawaki, T. Mochida, T. Sakurai, H. Ohta and K. Takahashi, *Inorg. Chem.*, 2020, **59**, 12295.
129. F. Rupp, K. Chevalier, M. Graf, M. Schmitz, H. Kelm, A. Grün, M. Zimmer, M. Gerhards, C. van Wüllen, H.-J. Krüger and R. Diller, *Chem. Eur. J.*, 2017, **23**, 2119.
130. H. Paulsen, V. Schünemann and J. A. Wolny, *Eur. J. Inorg. Chem.*, 2013, **1**, 628.
131. J. Sirirak, D. Sertphon, W. Phonsri, P. Harding and D. J. Harding, *Int. J. Quantum Chem.*, 2017, **117**, e25362.
132. O. S. Siig and K. P. Kepp, *J. Phys. Chem. A*, 2018, **122**, 4208.
133. D. Sato, Y. Shiota, G. Juhász and K. Yoshizawa, *J. Phys. Chem. A*, 2010, **114**, 12928.
134. A. A. Starikova and V. I. Minkin, *Russ. Chem. Rev.*, 2018, **87**, 1049.
135. S. Lebègue, S. Pillet and J. G. Ángyán, *Phys. Rev. B*, 2008, **78**, 024433.
136. S. Vela, M. Fumanal, J. Cirera and J. Ribas-Arino, *Phys. Chem. Chem. Phys.*, 2020, **22**, 4938.
137. N. Azzaroli, A. Lapini, M. Di Donato, A. Dei and R. Righini, *J. Phys. Chem. B*, 2013, **117**, 15492.
138. P. Tourón Touceda, S. Mosquera Vázquez, M. Lima, A. Lapini, P. Foggi, A. Dei and R. Righini, *Phys. Chem. Chem. Phys.*, 2012, **14**, 1038.
139. M. K. Biswas, S. C. Patra, A. N. Maity, S.-C. Ke, T. Weyhermüller and P. Ghosh, *Dalton Trans.*, 2013, **42**, 6538.
140. D. M. Adams, L. Noodleman and D. N. Hendrickson, *Inorg. Chem.*, 1997, **36**, 3966.
141. M. Kondo, M. Uchikawa, K. Namiki, W.-W. Zhang, S. Kume, E. Nishibori, H. Suwa, S. Aoyagi, M. Sakata, M. Murata, Y. Kobayashi and H. Nishihara, *J. Am. Chem. Soc.*, 2009, **131**, 12112.
142. A. A. Starikova, M. G. Chegerev, A. G. Starikov and V. I. Minkin, *Comput. Theor. Chem.*, 2018, **1124**, 15.
143. A. Dei, A. Feis, G. Poneti and L. Sorace, *Inorg. Chim. Acta*, 2008, **361**, 3842.
144. A. Bencini, C. A. Daul, A. Dei, F. Mariotti, H. Lee, D. A. Shultz and L. Sorace, *Inorg. Chem.*, 2001, **40**, 1582.
145. A. Droghetti and S. Sanvito, *Phys. Rev. Lett.*, 2011, **107**, 047201.
146. S. Klokishner, *Chem. Phys.*, 2001, **269**, 411.
147. O. Reu, S. Ostrovsky, S. Decurtins, S.-X. Liu and S. Klokishner, *Eur. J. Inorg. Chem.*, 2017, **2017**, 5356.

Encyclopedia of Inorganic and Bioinorganic Chemistry, Online © 2011–2021 John Wiley & Sons, Ltd.
This article is © 2021 John Wiley & Sons, Ltd.
This article was published in the *Encyclopedia of Inorganic and Bioinorganic Chemistry* in 2021 by John Wiley & Sons, Ltd.
DOI: 10.1002/9781119951438.eibc2785